



HAL
open science

Integrating a compressible multicomponent two-phase flow into an existing reactive transport simulator

Irina Sin, Vincent Lagneau, Jérôme Corvisier

► **To cite this version:**

Irina Sin, Vincent Lagneau, Jérôme Corvisier. Integrating a compressible multicomponent two-phase flow into an existing reactive transport simulator. *Advances in Water Resources*, 2017, 100, pp.62-77. 10.1016/j.advwatres.2016.11.014 . hal-01516810

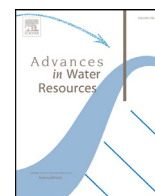
HAL Id: hal-01516810

<https://minesparis-psl.hal.science/hal-01516810>

Submitted on 2 May 2017

HAL is a multi-disciplinary open access archive for the deposit and dissemination of scientific research documents, whether they are published or not. The documents may come from teaching and research institutions in France or abroad, or from public or private research centers.

L'archive ouverte pluridisciplinaire **HAL**, est destinée au dépôt et à la diffusion de documents scientifiques de niveau recherche, publiés ou non, émanant des établissements d'enseignement et de recherche français ou étrangers, des laboratoires publics ou privés.



Integrating a compressible multicomponent two-phase flow into an existing reactive transport simulator



Irina Sin*, Vincent Lagneau, Jérôme Corvisier

MINES ParisTech, PSL Research University, Centre for Geosciences and Geoengineering, 35 rue Saint-Honoré, F-77305 Fontainebleau Cedex, France

ARTICLE INFO

Article history:

Received 15 March 2016

Revised 23 November 2016

Accepted 25 November 2016

Available online 27 November 2016

Keywords:

Compressible two-phase flow

Reactive transport

Sequential iterative coupling

Operator splitting

HYTEC

Equation of state

ABSTRACT

This work aims to incorporate compressible multiphase flow into the conventional reactive transport framework using an operator splitting approach. This new approach would allow us to retain the general paradigm of the flow module independent of the geochemical processes and to model complex multiphase chemical systems, conserving the versatile structure of conventional reactive transport. The phase flow formulation is employed to minimize the number of mass conservation nonlinear equations arising from the flow module. Applying appropriate equations of state facilitated precise descriptions of the compressible multicomponent phases, their thermodynamic properties and relevant fluxes.

The proposed flow coupling method was implemented in the reactive transport software HYTEC. The entire framework preserves its flexibility for further numerical developments. The verification of the coupling was achieved by modeling a problem with a self-similar solution. The simulation of a 2D CO₂-injection problem demonstrates the pertinent physical results and computational efficiency of this method. The coupling method was employed for modeling injection of acid gas mixture in carbonated reservoir.

© 2016 The Authors. Published by Elsevier Ltd.

This is an open access article under the CC BY-NC-ND license (<http://creativecommons.org/licenses/by-nc-nd/4.0/>).

1. Introduction

1.1. Background/motivation

Human activity in the subsurface has been expanding and diversifying (waste disposal, mining excavation and high-frequency storage of energy), and the public and regulatory expectations have been increasing. The assessment of each step of underground operations, including environmental impact evaluation, relies on elaborate simulators and leads to an urgent need to develop multiphysics modeling. Reactive transport, a geochemical research and engineering tool, is used in multicomponent systems and sophisticated chemical processes (activity and fugacity correction according to different models, mineral dissolution and precipitation, cation exchange, oxidation and reduction reactions, isotopic fractionation and filtration), in addition to gas evaporation and dissolution (van der Lee et al., 2003; Mayer et al., 2012; Parkhurst and Appelo, 1999; Steefel, 2009; Yeh et al., 2004). Multiphase flow is based on broad experiences in reservoir engineering research, including the thermodynamic modeling of complex phase behavior. In particular, the equations of state were used to simulate

and study interfacial tension, gas, steam and alkaline injection in oil reservoirs and enhanced oil recovery (Delshad et al., 2000; Farajzadeh et al., 2012; Nghiem et al., 2004; Wang et al., 1997).

This work aims to incorporate a compressible multiphase flow module into an existing reactive transport simulator. Our coupling method should therefore meet the following requirements:

1. The new approach should handle the different complex multiphase chemical models and retain the general paradigm of a multiphase flow module independent of the geochemical system and conserve the conventional reactive transport structure;
2. The number of mass conservation nonlinear equations arising from the flow module should be minimized such that the reduced flow system preserves the matrix structure and minimizes the computational intensity;
3. The entire framework should preserve its flexibility for possible non-isothermal, geomechanical and domain decomposition developments in the future.

Reactive transport methods have been extensively investigated over the past two decades (see below). This work focuses on the coupling between multicomponent multiphase flow (MMF¹) and

* Corresponding author.

E-mail address: irina.sin@mines-paristech.fr (I. Sin).

¹ The nomenclature is provided in Table 1. The abbreviations are detailed in Table 2.

Table 1
Nomenclature.

Latin symbols	
a_k	activity of potential catalyzing or inhibiting species
A_s	specific surface area, [m^2/m^3 solution] or [m^2/kg mineral]
$C_{l,k}$	total liquid mobile concentration of basis species k , [mol/kg w]
$C_{s,k}$	immobile concentration of basis species k , [mol/kg w]
$C_{g,m}$	gas concentration of basis species m , [mol/m^3]
C_i	concentration of primary species i in chemical module
d	dissolution parameter of transport model
dt	time step
D_α	molecular diffusion coefficient of phase α , [m^2/s]
D_α^e	effective diffusion coefficient of phase α , [m^2/s]
\mathbf{D}_α	diffusion-dispersion tensor of fluid phase α
e	evaporation parameter of transport model
f_i^α	fugacity of species i in phase α
\mathbf{F}	residual function
\mathbf{g}	gravitational acceleration vector, [m/s^2]
\mathbf{J}	Jacobian
k	number of iterations in flow coupling
k_{kin}	kinetic rate constant in , [$mol/m^2/s$]
k_{max}^l	maximum number of iterations in flow coupling
k_{max}^r	maximum number of iterations in reactive transport coupling
$k_{r\alpha}$	relative permeability of phase α
K	intrinsic permeability, [m^2]
\mathbb{K}	intrinsic permeability tensor, [m^2]
K_i	K-value/equilibrium ratio
K_j	equilibrium constant of reaction j
K_s	equilibrium solubility constant of solid phase
K_i^h	Henry's law constant
M	molar mass of species \cdot , [kg/mol]
n_α	quantity of matter in phase α
\mathbf{n}	normal vector
N_c	number of primary species in chemistry module
N_f	number of fluid phases α
N_g	number of gas species
N_{kin}	number of kinetic reactions
N_{Nit}	number of Newton iterations
N_{Pic}	number of Picard iterations
N_p	number of phases
N_r	number of independent chemical reactions
N_s	number of species in chemistry module
p_α	liquid/gas pressure, [Pa]
P	pressure, [Pa]
\mathbf{P}_c	set of the critical pressures
q_α	mass source term of phase α , [kg/s]
$q_{\alpha,k}$	mass source term of species k in phase α , [kg/s]
$q_{g,m}$	source term of basis species m in the gas phase, [mol/m^3]
$q_{l,k}$	source term of basis species k in the liquid phase, [mol/kg w]
Q_s	ion activity product
$T_{\alpha\beta}$	reaction term of phases α and β in α transport operator
R	gas constant, [$J/K/mol$]
R_α	reaction term of phase α , [kg/s]
$R_{\alpha,k}$	reaction term of species k in phase α , [kg/s]
$R_{g,m}$	reaction term of basis species m in the gas phase, [mol/m^3]
$R_{l,k}$	reaction term of basis species k in the liquid phase, [mol/kg w]
\mathbf{R}	geochemical reaction operator
S_j	concentration of species j in chemical module
S_α	saturation of phase α
t	calculation time of entire system per time step
t_{fl}	calculation time of flow operator per iteration
t_{fc}	calculation time of flow coupling per iteration
t_{gt}	calculation time of gas transport operator per iteration
t_{rtc}	calculation time of reactive transport coupling per iteration
T	temperature, °C and K
T_i	total concentration in chemistry module
\mathbf{T}_c	set of the critical temperatures
\mathbf{T}_α	transport operator of phase α
\mathbf{u}_α	Darcy's velocity of phase α
v	molar volume, [m^3/mol]
V_α	volume of porous space occupied by phase α , [m^3]
V_{tot}	total volume, [m^3]
x_i	mole fraction of basis species i in the liquid phase
$X_{\alpha,k}$	mass fraction of basis species k in phase α
\mathbf{x}	vector of primary variables of the flow system
y_i	mole fraction of basis species i in the gas phase

Table 1 (continued)

Latin symbols	
Z	compressibility factor
\mathbf{Z}_c	set of the critical compressibility factors
Greek symbols	
$\alpha = \{l, g\}$	liquid/gas phase
α_{ij}	stoichiometric coefficient
γ_j	activity coefficient
Δ	matrix of binary interaction coefficients of PR EOS
ϵ_g	gas quantity tolerance in reactive transport coupling
ϵ_{Nf}	residual function tolerance in flow coupling
ϵ_{qss}	quasi-stationary state tolerance in flow coupling
ϵ_{rt}	tolerance in reactive transport coupling
μ_α	viscosity of phase α , [$Pa \cdot s$]
ρ_α	mass density of phase α , [kg/m^3]
ρ_α^g	density of phase α in the gravity term, [kg/m^3]
τ_α	tortuosity of phase α
ϕ	porosity
ϕ_i^α	fugacity coefficient of species i in phase α
ψ_α	volumetric rate of phase α , [m^3/s]
Ξ	acentric factor set
Ω	mathematical transport operator of phase α
$\ \cdot \ _\infty$	infinity norm
$\mathbb{1}_{\mathbb{R},0}(\cdot)$	indicator function of the set of strictly positive real numbers

Table 2

Abbreviations.

AIM	adaptive implicit method
CFL	Courant-Friedrichs-Lewy number
DAE	differential algebraic equations based method
DSA	direct substitution approach
EOS	equation of state
FIM	fully implicit method
FVM	finite volume method
GIA	global implicit approach
IMPEC	implicit pressure/explicit concentration
MMF	multiphase multicomponent flow
MMRF	multiphase multicomponent reactive flow
ODE	ordinary differential equations based method
PDE	partial differential equation
OSA	operator splitting approach
RT	reactive transport
SI	saturation index
SIA	sequential iterative approach
SNIA	sequential non-iterative approach
TPFA	two-point flux approximation

reactive transport (RT) modules and starts by surveying the existing approaches

1.2. A review of multiphase multicomponent flow and reactive transport codes

1.2.1. Operator splitting algorithms between MMF and RT

The strength of the operator-splitting approach (OSA) (sequential iterative (SIA) or sequential non-iterative (SNIA)) arises from the framework flexibility, which allows each model to be developed and verified independently. These are important reasons for selecting the OSA for the coupling between MMF and RT, particularly when extending a hydrogeochemical code from single- to two-phase flow. The following codes apply the OSA: CodeBright (Olivella et al., 1996) (coupling with the reactive transport code RETRASO (Saaltink et al., 2004)), DuMu^X (based on DUNE) (Ahusborde et al., 2015; Vostrikov, 2014), DUNE (Hron et al., 2015), HYDROGEOCHEM (unsaturated) (Yeh et al., 2004, 2012), iCP (Nardi et al., 2014), IPARS (Peszynska and Sun, 2002; Wheeler et al., 2012), MIN3P (the bubble model) (Mayer et al., 2012; Molins and Mayer, 2007), MoReS (Farajzadeh et al., 2012; Wei, 2012), NUFT (Hao et al., 2012), PFLOTRAN (Lichtner et al., 2015; Lu and Lichtner, 2007),

STOMP (White et al., 2012; White and Ostrom, 2006), TOUGHREACT (Xu and Pruess, 1998; Xu et al., 2012), and UTCHEM (Delshad et al., 2000); see also (Steeffel et al., 2014).

The simulators are primarily based on the finite volume method (FVM) because of its conservative properties. The general tendency in coupling is to first (non-)iteratively solve the flow to obtain the velocities. The compositional formulation is typically chosen, or alternatively, the conservation equations can be solved for the dominant components (e.g., water/air). When the two-phase flow system involves only two components (e.g., H₂O and CO₂), the final sets of equations for the compositional and dominant component formulations are identical and reduce to the mass conservation for each component.

Once the flow is established, the RT part can be solved using the OSA (SIA, SNIA or predictor-corrector); a global implicit approach (GIA), such as the ordinary differential equation-based method (ODE, the chemistry module is used as a black box), the direct substitution approach (DSA) (Saaltink et al., 2001) or the differential algebraic equation-based method (DAE) (de Dieuleveult, 2008; de Dieuleveult et al., 2009). The OSA and GIA applied to RT are compared in Carrayrou et al. (2010); de Dieuleveult et al. (2009); Saaltink et al., (2001); Steffel and MacQuarrie (1996). In 2001, Saaltink et al. (2001) reported that SIA was more favorable than DSA in cases of large grids and low kinetic rates because of the high computer storage requirements and slow linear solvers. A decade later, the MoMaS benchmark confirmed the reliability of both approaches and the enhanced computational potential of the DSA with the reduction technique (Kräutle and Knabner, 2007).

1.2.2. From global implicit algorithm in RT to global implicit algorithm in MMF&RT

The advantage of GIA is its accuracy, although it comes at the cost of computational resources. However, this method is becoming more competitive because of increases in computer capabilities and advances in the methods that allow reducing the system of equations. Additionally, reservoir simulators typically utilize the global formulation for the MMF problem combined with the fully implicit method (FIM) or the adaptive implicit method (AIM), which unifies the FIM and implicit pressure/explicit concentration (IMPEC). They can therefore be naturally extended to the RT using GIA, e.g., COORES², GEM-GHG (Nghiem et al., 2004), GPAS (Pope et al., 2005), and GPRS (Cao, 2002; Fan et al., 2012).

For the global implicit solution of the RT, several techniques have been proposed to reduce the initial mass balance system by linear combination and eliminate the reaction terms in the equilibrium reactions (Kräutle and Knabner, 2007; Molins et al., 2004; Saaltink et al., 1998). Such modifications of the DSA for RT lead to mathematical decoupling of the entire system and consequently make it interesting for the global implicit coupling of multiphase flow and reactive transport, as recently demonstrated by Saaltink et al. (2013) and Fan et al. (2012). Saaltink et al. (2013) proposed a method for introducing the chemistry calculations to a conventional multiphase simulator to minimize the number of mass conservation equations by taking the fluid phase pressures and porosity as primary variables and expressing all secondary variables (such as component concentrations, fugacity, pH, and salinity) as a polynomial function of gas pressure, which requires pre-processing prior to each application. Fan et al. (2012) employed the element balance formulation (Michelsen and Mollerup, 2007) via reduction techniques (Kräutle and Knabner, 2007; Molins et al., 2004) and the decoupled linearized system on the primary and secondary equations. Saaltink et al. (2013) demonstrated that the GIA and OSA provided similar results for CO₂ storage and concluded that the full coupling was not necessary for MMF&RT modeling from a

physical perspective, although the OSA can be more computationally expensive.

Moreover, Gamazo et al. (2012) highlighted the significant impact of geochemical reactions on the phase fluxes by modeling gypsum dehydration when the non-isothermal flow is chemically restrained, i.e., the anhydrite-gypsum paragenesis controls the water activity and hence the evaporation process. The importance of DSA, which implicitly connects the equilibrium heterogeneous reactions and the phase flow, was emphasized compared with the decoupled formulation of the flow and the RT: the decoupled formulation overestimates the evaporation, but its computational time was reduced by 22.5% (compared to DSA). However, the definitions of water activity and liquid density were different in the GIA's and OSA's models. Furthermore, the decoupled flow system contained the conservation equations for dominant components (water and air), but the coupling between flow and RT was not specified. Given the nature of the formulations described in this work, it is likely that using the strong OSA (the SIA-based connection between flow and RT with the precise reaction terms in flow equations) would yield results similar to those of DSA at the cost of additional iterations.

1.3. Preamble to a new MMF&RT coupling approach

To reduce the number of nonlinear equations arising from the flow system, the formulation of the dominant components was considered. This approach is efficient when the impact of the other species is negligible. In geochemical problems, the speciation can vary largely over time and space. Ideally, the dominant components should be adapted locally to preserve the accuracy, but this would require specific treatment of the global flow solution.

If the flow system expands such that many species play significant roles in the thermodynamic state and phase displacement, then the number of nonlinear equations of compositional flow increases with the number of components, which is computationally expensive.

Despite the reduction techniques, the primary nonlinear system must be calculated. In geochemical modeling, which includes complex homogeneous and heterogeneous reactions, the primary (basis) species typically changes spatially and temporally. The system of equations is therefore redefined, which requires modifications of the Jacobian structure within Newton's method. The solution of the transport linear system can be several or even a hundred times faster than that of multiphase flow.

To minimize the size of the nonlinear system, it is possible to replace the compositional formulation by the phase formulation. The phase flow coupled to the RT was employed by Peszynska and Sun (2002). Given their problem conditions (slightly compressible fluids and density-independent flow), the authors divided the RT into three stages (advection, reaction, and diffusion) within the internal time steps by interpolating the fluxes and saturations. Later, Hron et al. (2015) simulated *Escherichia coli* growth and transport under aerobic and anaerobic conditions via the sequential coupling of phase flow and the SNIA-based RT. The liquid fluid was assumed to be incompressible, whereas the gas density was composition dependent. In the advective-dominant regime, the transport was solved explicitly in a time that led to a time step restriction: CFL = 0.4; thus, the split transport time step was applied. Note that the same issue arises from the IMPEC scheme in which the component equations are solved explicitly.

1.4. Our alternative method

This work proposes a new approach for incorporating the compressible two-phase flow in a conventional reactive transport simulator. It is based on the phase flow formulation and preserves all

² A. Michel and T. Faney, personal communication, 2015

the sustainability and facilities of the reactive part. This method builds on the unconditional stability of the fully implicit scheme and can model advective-dominant and density-driven regimes.

The following simplifications are considered in this work: isothermal flow and no geomechanics. The method was applied to the (SIA) reactive transport simulator HYTEC (Lagneau and van der Lee, 2010b; van der Lee et al., 2003). The HYTEC code has been widely evaluated in several benchmark studies (Carrayrou et al., 2010; Lagneau and van der Lee, 2010a; Trotignon et al., 2005; de Windt et al., 2003) and numerous applications, such as cement degradation (de Windt and Devillers, 2010), radioactive waste disposal (Debure et al., 2013; de Windt et al., 2014), geological storage of acid gases (Corvisier et al., 2013; Jacquemet et al., 2012; Lagneau et al., 2005), and uranium in situ recovery processes (Regnault et al., 2014).

In Section 2, a concise description of the governing equations of multicomponent multiphase flow and reactive transport is given. Next, the proposed coupling methods are detailed in Section 3. Section 4 presents the method's applicability and computational performance, first using a benchmark problem with a self-similar solution and then for modeling 2D CO₂ injection. Section 4 also illustrates a problem of acid gas injection in carbonated reservoir. The conclusions are presented in Section 5.

2. Governing processes and mathematical formulation

The standard entire isothermal MMRF problem is composed of component $c_{\alpha,k}$ mol conservation, mass balance, mass-action laws and other constitutive relations. The total number of phases is $N_p = 3$, where the solid phase is immobile and the N_f fluid phases α are mobile (liquid and gas). The chemical system of N_s chemical species and N_r linearly independent chemical reactions relies on Morel's method (Morel and Hering, 1993) of N_c primary species that form a basis for all N_s species: $N_c = N_s - N_r$.

2.1. Mass conservation for each phase

We first introduce the standard multiphase compositional flow problem and the physical parameters, and then we present the phase mass conservation formulation and its advantages. Let us begin with the general mass conservation in terms of the mass fraction $X_{\alpha,k}$ of species k in fluid phase α that forms $N_c N_f$ equations:

$$\frac{\partial(\phi S_{\alpha} \rho_{\alpha} X_{\alpha,k})}{\partial t} = -\nabla \cdot (\rho_{\alpha} X_{\alpha,k} \mathbf{u}_{\alpha} - \rho_{\alpha} \mathbf{D}_{\alpha} \nabla X_{\alpha,k}) + R_{\alpha,k} + q_{\alpha,k}, \quad (1)$$

where ϕ is the porosity, S_{α} is the saturation of fluid phase α , ρ_{α} is the mass density of fluid phase α , \mathbf{u}_{α} is the Darcy-Muskat velocity of fluid phase α , \mathbf{D}_{α} is the diffusion-dispersion tensor of fluid phase α . The classical Fick's law is used for the diffusion coefficients D_{α} that are then scalar and independent of composition; for each phase α , the diffusion coefficient should be identical for all species to preserve the consistency of system (Hoteit, 2011). In this work, the dispersion term is neglected. Consequently, the diffusion-dispersion tensor \mathbf{D}_{α} transforms into the effective diffusion $D_{\alpha}^e = \phi S_{\alpha} D_{\alpha}$. $R_{\alpha,k}$ is the reaction term, and $q_{\alpha,k}$ is the external source term of species k in fluid phase α . The Darcy-Muskat law (Muskat et al., 1937) states that

$$\mathbf{u}_{\alpha} = -\frac{k_{r\alpha}}{\mu_{\alpha}} \mathbb{K}(\nabla p_{\alpha} - \rho_{\alpha} \mathbf{g}), \quad (2)$$

where $k_{r\alpha}$, μ_{α} and p_{α} are the relative permeability, viscosity and pressure of fluid phase α , respectively. \mathbb{K} is the intrinsic permeability tensor, and \mathbf{g} is the gravitational acceleration vector. The pressures are connected by $N_f - 1$ capillary pressure relations, and the saturations and mass fractions sum to 1:

$$\sum_{\alpha} S_{\alpha} = 1, \quad (3)$$

$$\sum_k X_{\alpha,k} = 1. \quad (4)$$

Thus, an additional $2N_f$ constitutive relations are generated. The conventional PDE system of isothermal compositional multiphase flow can be expressed using (1) by deriving the conservation of each species k in all phases Σ_{α} . These N_c nonlinear equations, $2N_f$ constitutive relations and $N_c(N_f - 1)$ phase equilibrium relations (Section 2.3) yield $2N_f + N_c N_f$ equations for $2N_f + N_c N_f$ unknowns p_{α} , S_{α} and $X_{\alpha,k}$. According to the Gibbs phase rule, the number of intensive properties is $N_c - N_p + 2$. If the number of phases is locally known, then $N_p = 2$ for fixed temperature, and at least N_c nonlinear equations (e.g., pressure and composition (Jindrová and Mikyška, 2015)) can be solved to establish the thermodynamic state. Note that the geochemical system can be abundant in species, implying that considerably large nonlinear systems must be solved.

In this work, we propose handling a phase mass conservation system of N_f PDE whose size is independent of the number of chemical species N_s . We apply Σ_k to (1) to obtain

$$\frac{\partial(\phi S_{\alpha} \rho_{\alpha})}{\partial t} = -\nabla \cdot (\rho_{\alpha} \mathbf{u}_{\alpha}) + R_{\alpha} + q_{\alpha}, \quad (5)$$

taking into account that the sum of diffusive fluxes for each phase α is equal to 0 because the diffusion coefficients D_{α} are equal over all components in each phase. The external source term q_{α} can also be presented as

$$q_{\alpha} = \rho_{\alpha} \psi_{\alpha}, \quad (6)$$

where ψ_{α} is the volumetric rate. The system (5) of N_f equations, $N_f - 1$ capillary pressure relations and (3) is assembled for $2N_f$ unknowns, p_{α} and S_{α} , which are natural variables of multiphase flow problems.

When one of the phases disappears, the corresponding equation of system (5) degenerates, and the natural variables are no longer appropriate for describing the system. In this case, we move to the single-flow problem. Numerous formalisms are dedicated to the two-component, two-phase flow and associated phase disappearance/appearance (Abadpour and Panfilov, 2009; Angelini et al., 2011; Bourgeat et al., 2013; Lauser et al., 2011; Masson et al., 2014; Pruess et al., 1999). In this work, the liquid phase is assumed to be present throughout the system, even if it is present in small amounts. The liquid pressure and gas saturation are chosen as primary variables. Therefore, solving the system of N_f nonlinear Eq. (5) can be beneficial when $N_c > N_f$. Although a semi-implicit method IMPEC is used to reduce the number of nonlinear equations to be solved simultaneously (Hoteit and Firoozabadi, 2006; Mikyška and Firoozabadi, 2010), time stepping is constrained by the CFL condition. Alternatively, an implicit method of decoupled system has been proposed in Zidane and Firoozabadi (2015). The authors solve implicitly the species transport coupled with the total flux calculated by the mixed finite element method.

2.2. Mole conservation for each gas component and primary species

The liquid and gas phases consist of N_c primary species and N_g gas species, respectively, $N_g < N_c$, for which the transport must be solved. We chose the transport formulation in terms of concentrations $c_{\alpha,k} = \rho_{\alpha} X_{\alpha,k} / M_k$, where M_k is the molar mass of species k . Deriving the transport equations in mole/mass fractions, as in Eq. (1), the density deviation $\nabla \rho_{\alpha} / \rho_{\alpha}$ that arises from the diffusive part of flux is neglected. Based on the primary species formalism (van der Lee, 2009; Lichtner, 1996; Steefel and MacQuarrie, 1996; Yeh and Tripathi, 1991), the liquid transport is defined for the total

liquid mobile concentration $c_{l,k}$ of primary species k and the gas transport for the gas concentration $c_{g,m}$ of gas species m , which yields $N_c + N_g$ transport (linear) equations:

$$\frac{\partial \phi S_l c_{l,k}}{\partial t} = -\mathfrak{T}_l(c_{l,k}) + R_{l,k}(c_{l,k}, c_{s,k}) + q_{l,k}, \quad (7)$$

$$\frac{\partial \phi S_g c_{g,m}}{\partial t} = -\mathfrak{T}_g(c_{g,m}) + R_{g,m}(c_{g,m}) + q_{g,m}, \quad (8)$$

where $c_{s,k}$ is the immobile concentration of species k , operator \mathfrak{T}_α includes the advective flux presented by the Darcy–Muskat law (2), and assuming non-Knudsen diffusion, Fick's law for diffusive flux yields (Lichtner, 1996; de Marsily, 2004):

$$\mathfrak{T}_\alpha(c_{\alpha,k}) = \nabla \cdot (c_{\alpha,k} \mathbf{u}_\alpha - D_\alpha^e \nabla c_{\alpha,k}), \quad (9)$$

where D_α^e can involve the tortuosity coefficient τ_α (Millington and Quirk, 1961).

2.3. Mole balance for each primary basis species

The chemical equations arise from the mass action law and phase equilibrium relations. As mentioned above, the reactive transport code is based on the primary species formulation, and thus, we denote the concentration of species S_j , $j = 1, \dots, N_s$, that can be expressed as a function of basis species C_i , $i = 1, \dots, N_c$:

$$S_j = \sum_{i=1}^{N_c} \alpha_{ij} C_i, \quad (10)$$

where α_{ij} is the stoichiometric coefficient. At equilibrium, the mass action law provides the reaction affinity:

$$S_j = \frac{K_j}{\gamma_j} \prod_{i=1}^{N_c} (\gamma_i C_i)^{\alpha_{ij}}, \quad (11)$$

where γ_j is the activity coefficient and K_j is the thermodynamic equilibrium constant of reaction j . All aqueous reactions are considered to be at equilibrium. For each basis species, the mole balance can be written in terms of the total concentration T_i , $i = 1, \dots, N_c$, $T_i = \sum_{j=1}^{N_s} \alpha_{ji} S_j$,

$$T_i - C_i - \sum_{j=1, j \neq i}^{N_c} \alpha_{ji} \frac{K_j}{\gamma_j} \prod_{i=1}^{N_c} (\gamma_i C_i)^{\alpha_{ij}} = 0, \quad (12)$$

constituting a system of N_c equations on C_i , $i = 1, \dots, N_c$.

2.3.1. Liquid mixtures

In non-ideal liquid mixtures, the activity coefficients γ_i are not trivial and can be calculated using different models whose complexity increases with the concentration of solution, from less to more concentrated solution: truncated Davies formula (Colston et al., 1990), B-dot (Helgeson, 1969), SIT (Grenthe et al., 1997), and Pitzer (1991).

2.3.2. Gas-liquid equilibrium

The chemical potentials and corresponding fugacities of species i in mixture f_i^α are equal under equilibrium conditions. The fugacity-activity ($\varphi - \gamma$) approach yields

$$P y_i \varphi_i^g = f_i = K_i^h \gamma_i x_i, \quad (13)$$

where y_i is the mole fraction of species i in the gas phase, φ_i^g is the fugacity coefficient of species i , $K_i^h = K_i^h(T, P)$ is the corrected Henry's constant of species i , γ_i is the asymmetric activity coefficient of species i (Michelsen and Mollerup, 2007), and x_i is the mole fraction of species i in the liquid phase. K_i^h includes the Poynting factor, which corrects the reference fugacity with respect to the pressure and is near unity at low to moderate pressures.

The fugacity coefficients can be calculated using the equation of state (EOS). We chose the Peng–Robinson EOS (Robinson and Peng, 1978), which precisely reflects the gas mixture properties at high pressures/temperatures. For a given P , the cubic equation should be solved for the compressibility factor $Z = Pv/RT$, where v is the molar volume. The fugacity coefficient is then calculated as follows (Robinson and Peng, 1978): $\varphi_i^g = \varphi_i^g(T, P, Z, \mathbf{T}_c, \mathbf{P}_c, \mathbf{Z}_c, \mathbf{\Omega}, \mathbf{\Delta})$, where \mathbf{T}_c , \mathbf{P}_c , and \mathbf{Z}_c are the sets of the critical temperatures, critical pressures and compressibility factors of the species in the mixture, respectively. $\mathbf{\Omega}$ is the acentric factor set, and $\mathbf{\Delta}$ is the matrix of empirical binary interaction parameters for each pair of species in the mixture.

The EOS also provides the mass density for gas mixtures:

$$\rho_g = \frac{\sum_{i=1}^{N_g} y_i M_i}{v} = \frac{\bar{M}}{v}, \quad (14)$$

and, by analogy, for liquid mixtures: $\bar{M} = \sum_{i=1}^{N_c} x_i M_i$.

Note that Raoult's law ($P y_i = P^{sat} x_i$) is derived from Eq. (13), assuming low pressure conditions and ideal solutions.

2.3.3. Liquid-solid equilibrium and kinetic relations

For minerals under the thermodynamic equilibrium assumption, the solubility constant K_s can be derived from the mass action law. The mineral activity is unity by convention. By omitting the index j , Eq. (11) yields the expression for the equilibrium solubility constant for solid s

$$K_s = \prod_{i=1}^{N_c} (\gamma_i C_i)^{\alpha_{ij}}. \quad (15)$$

When the reactions are kinetically controlled, the rate law can be described, e.g., by the transition state theory (Lasaga, 1984). The model uses the ion activity product Q_s , which by definition becomes K_s at equilibrium, and the saturation index (SI):

$$SI = \log \left(\frac{Q_s}{K_s} \right) = \begin{cases} < 0 & \text{undersaturated} \rightarrow \text{dissolution,} \\ = 0 & \text{saturated} \rightarrow \text{equilibrium,} \\ > 0 & \text{oversaturated} \rightarrow \text{precipitation.} \end{cases} \quad (16)$$

Under the transition state theory, the kinetic rate law is then

$$\frac{dS}{dt} = A_s k_{kin} \left(\text{sign}(SI) \left(\left(\frac{Q_s}{K_s} \right)^{b_1} - 1 \right) \right)^{b_2} \prod_k a_k^{n_k} \quad (17)$$

where A_s is the specific surface area; k_{kin} is the kinetic dissolution/precipitation rate constant; b_1 , b_2 , and n_k are fitting parameters; and a_k is the activity of the potential catalyzing or inhibiting species.

The mole balance equations with the mass action laws for the species at equilibrium, the rate laws for kinetically limited solids and phase equilibrium relations constitute a complete system of algebro-differential equations whose solution yields the concentrations of basis and secondary species. Other chemical reactions can also be handled by the formalism of basis species, e.g., cation exchange and surface and organic complexation.

3. Numerical solution

Applying the OSA to subsurface environmental modeling enables the independent development of separated modules of code and the rigorous solution of each. Consequently, the majority of RT simulators rely on the OSA (Steeffel et al., 2014). The assessment of different coupling methods was studied for the MoMaS benchmark of RT codes (Carrayrou et al., 2010; Carrayrou and Lagneau, 2007), during which the reliabilities of both the SIA and GIA were determined, and the detailed results of HYTEC were reported in Lagneau and van der Lee (2010a). Following the general strategy of integrating the (un)saturated flow in RT codes by OSA, we solved

the compressible two-phase flow block first. This process involved the flow system, the gas transport equations, and the EOS and fluid property models. Then, reactive transport coupling was applied. We propose employing SIA for each module, and hence, two internal SIA-based couplings exist. Let us describe the applied methods for flow and transport discretization and the subsequent coupling methods.

3.1. Discretization of flow and transport

The discretization of mass phase conservation (5) and mole species transport (7), (8) is constructed based on a Voronoi-type finite volume method. The time approximation of two-phase flow (5) is fully implicit, and the fluxes are handled by TPFA. In the 1960s, the transmissibility discretization was demonstrated to affect the numerical stability and accuracy (Allen, 1984; Blair and Weinaug, 1969; Settari and Aziz, 1975); in this work, the interface coefficients of flow between adjacent cells were evaluated implicitly and upstream. For the relative permeability $(k_{r\alpha})_{ij}$, the upstream space approximation is widely used because its convergence was confirmed for the Buckley–Leverett problem (Aziz and Settari, 1979; Bastian, 1999). The detailed comparison of temporal discretization presented in Aziz and Settari (1979); Blair and Weinaug (1969) demonstrated the stability advantages of the implicit upstream treatment relative to explicit ones but also reported increased truncation errors. We will discuss the impact of truncation errors in Section 4.1. The relative permeability $k_{r\alpha}$, intrinsic permeability K , phase density ρ_α , and phase viscosity μ_α of the interface coefficients between adjacent cells i, j at iteration $k+1$ are therefore defined as

$$(\cdot)_{ij}^{k+1} = \begin{cases} (\cdot)_i^k & \text{if } \mathbf{u}_\alpha^k \mathbf{n}_{ij} > 0, \\ (\cdot)_j^k & \text{else} \end{cases} \quad (18)$$

where \mathbf{n}_{ij} is the normal vector from i to j .

The discretization of density $(\rho_\alpha^g)_{ij}$ in the gravity term $\rho_\alpha \mathbf{g}$ is treated differently and weighted relative to the effective phase volume. If the gas phase is absent in one of the cells, then the upstream treatment is applied (Coats, 1980):

$$(\rho_\alpha^g)_{ij} = \begin{cases} \rho_{\alpha,i} \sigma + \rho_{\alpha,j} (1 - \sigma) & \text{if } (S_{\alpha,i} > 0) \wedge (S_{\alpha,j} > 0) : \\ & \sigma = V_{\alpha,i} / (V_{\alpha,i} + V_{\alpha,j}); \\ (\rho_\alpha)_{ij} & \text{else} \end{cases} \quad (19)$$

where $V_\alpha = \phi S_\alpha V_{tot}$ and V_{tot} is the volume of the cell. The resulting nonlinear system can be solved using Newton's method with an analytical Jacobian, as presented in Section 3.2.

The space discretization of transport operators (7) and (8) is achieved by upstream weighting for advective flux and harmonic weighting for effective diffusion. The semi-implicit method is chosen for the time discretization: the implicit Euler scheme is applied for the diffusive flux, whereas the advective part is discretized using the Crank–Nicolson method.

3.2. Coupling 1: compressible two-phase flow

Because the phase flow system (5) is nonlinear, the classic Newton's method is applied. We denote the discretized Eq. (5) as $\mathbf{F}(\mathbf{x}) = 0$, where $\mathbf{x} = (\mathbf{p}, \mathbf{S}_g)$. When the fluids are highly compressible (e.g., the gas phase), the density properties should be precisely evaluated at each deviation of the intensive variables P, V , and n , where n is the quantity of matter. To ensure the implicit treatment of interface coefficients, the density is updated in Newton's loop, similar to the other flow parameters. However, the gas density may be strongly dependent on its composition. Therefore, the gas composition must be calculated by employing the gas transport (8) denoted by $\mathbf{T}_g(\mathbf{c}_g; \mathbf{x}) = 0$. This is particularly important for

modeling the gas appearance and disappearance. The flow coupling algorithm for time step $n+1$ is presented in Algorithm 1, and its parsing is given below.

Algorithm 1 Newton's method for flow.

```

1:  $\varepsilon_{Nf} = 1 \times 10^{-6}$ 
2:  $\varepsilon_{qss} = 1 \times 10^{-24}$ 
3:  $k_{max}^{fl} = 9$ 
4:  $k = 0$ 
5: while  $(\|\mathbf{F}(\mathbf{x}^k)\|_\infty \geq \varepsilon_{Nf} \|\mathbf{F}(\mathbf{x}^0)\|_\infty) \wedge (\|\mathbf{F}(\mathbf{x}^k)\|_\infty \geq \varepsilon_{qss})$ 
    $\wedge (k \leq k_{max}^{fl})$  do
6:   find  $\delta \mathbf{x}^{k+1}$ :  $\mathbf{J}(\mathbf{x}^k) \delta \mathbf{x}^{k+1} = -\mathbf{F}(\mathbf{x}^k)$ 
7:    $\mathbf{x}^{k+1} \leftarrow \mathbf{x}^k + \delta \mathbf{x}^{k+1}$ 
8:   find  $\mathbf{c}_g^{k+1}$ :  $\mathbf{T}_g(\mathbf{c}_g^{k+1}; \mathbf{x}^{k+1}) = 0$ 
9:   update EOS and physical parameters
10:   $k \leftarrow k + 1$ 
11: end while

```

The user-defined or default tolerance ε_{Nf} (Section 3.4.3) and maximum number of Newton iterations k_{max}^{fl} for the flow coupling are initialized first. Next, the linearized system is solved for the increment $\delta \mathbf{x}$ at line 6. All the partial derivatives involved in the Jacobian \mathbf{J} of the discretized flow system are analytical. For example, the derivative of the gas density interface coefficient is expressed as

$$\frac{\partial (\rho_g)_{ij}}{\partial p_{g,i}} = \frac{\partial (\rho_g)_{ij}}{\partial \rho_{g,i}} \frac{\partial \rho_{g,i}}{\partial p_{g,i}}, \quad \frac{\partial \rho_{g,i}}{\partial p_{g,i}} = -\frac{\bar{M}_i}{v_i^2 (\partial p_g / \partial v)_i}, \quad (20)$$

where $\partial p_g / \partial v$ is the analytical derivative arising from the corresponding EOS. Note that the density derivatives are composition dependent and proportional to the average molecular weight \bar{M} and the density function Eq. (14). Various methods exist for solving multiphase systems of linear equations (Chen et al., 2006); we apply GMRES (Saad and Schultz, 1986), which is one of the most prevalent and efficient methods, with ILU(0) (van der Vorst and Meijerink, 1981) as a preconditioner.

Using the velocities and saturations given by \mathbf{x}^{k+1} from step 7, the linear transport system $\mathbf{T}_g(\mathbf{c}_g^{k+1}; \mathbf{x}^{k+1}) = 0$ is solved for \mathbf{c}_g^{k+1} at line 8 with GMRES and ILU(0). Because of the modified composition, the EOS parameters must be updated to evaluate a new molar volume v by solving the EOS analytically. Then, the physical properties can be calculated at line 9. Thereafter, three stop criteria must be checked at line 5: two for the flow system residual and one for the number of iterations.

The proposed coupling in Algorithm 1 corresponds to Newton's family for the flow system regarding \mathbf{x}^{k+1} , whereas it can be considered as Picard's method (fixed-point method) for the transport equations on \mathbf{c}_g^{k+1} . Given that the gas phase is supposed to be compressible and that significant differences in gas density may occur throughout the modeled domain, an additional criterion for gas quantity n_g deviation can be included:

$$\max \frac{|n_g^{k+1} - n_g^k|}{n_g^{k+1}} \leq \varepsilon_g, \quad (21)$$

where \max is the maximum value over the modeled domain. After numerous tests, we deduce that this may not be a necessary condition but is sufficient to finish the loop that depends on the complexity of gas dynamics. Despite neglecting the criterion (21), the solution's accuracy is not lacking. In addition, the reactive transport coupling described in Section 3.3, which follows the flow coupling in Algorithm 1, entails the convergence (stop) conditions for the gas and solid phases and guarantees the conservation of the entire system.

An adaptive time stepping is implemented for the relaxed CFL condition, number of Newton iterations and maximum saturation/pressure changes. Extremely large time steps are not reasonable, even if the scheme is unconditionally stable. Moreover, the subsequent reactive transport may require a smaller time step. In this case, smaller inner time stepping is commonly used. However, when the RT coupling is finished, the aggressive chemistry can yield important changes and provide large reaction terms and strong phase modifications of the flow block at the next time step. As a result, the flow solution deviates further from the first guess, and consequently, the convergence rate should decrease because it is quadratic only near the root. This issue will be discussed in Section 3.4.2.

Note that there is no calculation of the geochemical reactions in the flow coupling, but the reaction term R_α can be simply expressed as:

$$R_\alpha^n = \frac{(V_\alpha \rho_\alpha)^{n,rt} - (V_\alpha \rho_\alpha)^{n,fl}}{t^{n+1}}, \quad (22)$$

where t^n is time step n and $(\cdot)^{n,fl}$ and $(\cdot)^{n,rt}$ denote the values obtained by the flow and reactive transport couplings, respectively. The reaction terms are then estimated a posteriori at each time step, and the mass conservation is retained throughout the calculations. Additionally, note that when three phases (g, l, s) are included in the system, the term R_g reflects not only the gas and liquid connection but also the implicit gas-liquid-solid mass transfer, which is not negligible in conventional geochemical modeling. The precipitation and dissolution of some minerals can lead to gas depletion or formation, which affects saturation and pressure. These phenomena were numerically demonstrated in Gamazo et al. (2012). Consequently, the value of the reaction term can be highly important depending on the physical and chemical problem statement and the desired accuracy; e.g., in Vostrikov's work (Vostrikov, 2014), the reaction terms between the flow of dominant components and the reactive transport were neglected given the following assumptions: "only very small amounts of minerals are transferred to the liquid form" and "minor components do not have a significant impact on the physical parameters of system".

Algorithm 1 constitutes a simple two-phase system, where the gas concentrations are assumed to be the secondary variables, as for the relative permeability, the capillary pressure, and others. In this coupling, the flow can be fully unreactive if the gas displacement is the dominant mechanism and if the phase equilibrium calculations are taken explicitly, from the reactive transport coupling in this case.

3.3. Coupling 2: reactive transport

Relying on Algorithm 1 allows finding the phase velocities and saturations and consequently managing the reactive transport problem, which consists of the linear transport and nonlinear chemical equations. Analogous to the standard coupling in saturated porous media, Picard's method can be employed. On the one hand, the gas and liquid transport can be summed and written for each species, similar to GIA for multiphase multicomponent flow (Class et al., 2002; Lauser et al., 2011; Lichtner, 1996), by applying phase (dis-)appearance criteria and K-values $K_i = y_i/x_i$. In this work, this would be $K_i = K_i^h \gamma_i / (P \varphi_i^g)$, as derived from (13). In the non-ideal approach, γ_i is explicitly calculated for the electrostatic states of ions based on the ionic strength, as discussed in Section 2.3.1. Furthermore, φ_i^g is the function of the properties of the entire mixture, including y_i itself. Thus, K_i depends on both the aqueous and gaseous compositions and should be updated at each iteration as secondary variables. On the other hand, when solving the liquid (7) and gas (8) operators separately, the gas concentration from Algorithm 1 can be applied as a first guess, thereby

avoiding the need to calculate the K-value by introducing the reaction terms. By denoting transport operators as $T_\alpha(\mathbf{c}_\alpha) = 0$ and geochemical reaction modeling, as described in Section 2.3 by $\mathbf{R}(\mathbf{c})$, where $\mathbf{c} = \{\mathbf{c}_l, \mathbf{c}_g, \mathbf{c}_s\}$, we propose the SIA-based reactive transport Algorithm 2.

Algorithm 2 Picard's method for reactive transport.

```

1:  $\varepsilon_{rt} = 1 \times 10^{-5}$ 
2:  $k_{\max}^{rt} = 60$ 
3:  $k = -1$ 
4: while  $\left[ \left( \max \frac{|c_g^{2k+2} - c_g^{2k}|}{c_g^{2k+2}} \geq \varepsilon_{rt} \right) \vee \left( \max \frac{|c_s^{2k+2} - c_s^{2k}|}{c_s^{2k+2}} \geq \varepsilon_{rt} \right) \right] \wedge$ 
    $(k \leq k_{\max}^{rt})$  do
5:    $k \leftarrow k + 1$ 
6:    $T_g(\mathbf{c}_g^{2k+1}) = 0$ 
7:    $T_l(\mathbf{c}_l^{2k+1}) = 0$ 
8:    $\mathbf{c}^{2k+2} = \mathbf{R}(\mathbf{c}^{2k+1})$ 
9: end while

```

Let us establish the specific aspects of Algorithm 2. The reaction term r_{gl} , which is devoted to replicating the dissolution and evaporation rates, is introduced in the gas transport operator at line 6. Omitting the porosity and external sources, it can be formulated for gas species i as

$$\frac{S_g^{n+1} c_{g,i}^{n+1,2k+1} - S_g^n c_{g,i}^n}{t^{n+1}} = -(\mathfrak{T}_{g,i})_h + \frac{S_g^{n+1}}{t^{n+1}} r_{gl,i}^{n+1,2k+1}, \quad (23)$$

$$r_{gl,i}^{n+1,2k+1} = d_i^{n+1,2k} c_{g,i}^{n+1,2k+1} + e_i^{n+1,2k}, \quad (24)$$

where $(\cdot)_h$ denotes the discretization and $d_i^{n+1,2k}$ and $e_i^{n+1,2k}$ reflect the dissolution and evaporation processes, respectively. The terms $d_i^{n+1,2k}$ and $e_i^{n+1,2k}$ are calculated at the previous iteration $2k$, whereas $r_{gl,i}^{n+1,2k+1}$ corresponds to iteration $2k+1$. Considering the concentrations obtained in the previous iterations $\{1, \dots, 2k\}$, these parameters are defined as

$$d_i^{n+1,2k} = \sum_{m=1}^k \mathbb{1}_{\mathbb{R}_{>0}}(\Delta c_{g,i}^{n+1,2m}) \frac{\Delta c_{g,i}^{n+1,2m}}{c_{g,i}^{n+1,2m}}, \quad (25)$$

$$e_i^{n+1,2k} = \sum_{m=1}^k \mathbb{1}_{\mathbb{R}_{\leq 0}}(\Delta c_{g,i}^{n+1,2m}) \Delta c_{g,i}^{n+1,2m}, \quad (26)$$

where

$$\Delta c_{g,i}^{n+1,2m} = c_{g,i}^{n+1,2m} - c_{g,i}^{n+1,2m-1} \quad (27)$$

and $\mathbb{1}_{\mathbb{R}_{>0}}(\cdot)$ is the indicator function of the set of strictly positive real numbers. Note that the dissolution and evaporation processes are differently modeled. The asymmetric treatment is applied to avoid negative concentrations when dissolution leads to the total component consumption. Eq. (23) is still linear and can be directly solved by a linear solver, such as GMRES with ILU(0). This new distribution of gas species i entails different mass transfer that is likely associated with the corresponding total liquid mobile concentration of primary species j . Then, the liquid transport operator Eq. (7), line 7, is defined by

$$\frac{S_l^{n+1} c_{l,j}^{n+1,2k+1} - S_l^n c_{l,j}^n}{t^{n+1}} = -(\mathfrak{T}_{l,j})_h + \frac{S_l^{n+1}}{t^{n+1}} r_{lg,j}^{n+1,2k+1} + R_{ls,j}(c_{s,j}), \quad (28)$$

$$r_{lg,j}^{n+1,2k+1} = \sum_i \alpha_{ij} r_{gl,i}^{n+1,2k+1}, \quad (29)$$

where $R_{ls,j}$ is the reaction term of the liquid-solid interaction whose detailed description and variable porosity management are described in Lagneau and van der Lee (2010b).

After the transport, the reactive module is used to find a new local equilibrium state in line 8. The nonlinear chemical system for basis species is solved at each cell by Newton's method with the line-searching procedure. The Jacobian is then analytically evaluated. To improve the convergence, a new basis can be chosen independently in each cell; consequently, the set of primary equations also changes. Finally, the changes in the gas and solid concentrations are subjected to stop criterion verification in line 4 if the phase interactions (liquid–gas and liquid–solid) occur.

3.4. Coupling between compressible two-phase flow and reactive transport

3.4.1. Fully implicit scheme

To solve the phase flow formulation (5) rather than the compositional problem, other coupling approaches were also tested, including the following: Step 1. the phase conservation system to trace the first estimation of velocities and saturations; Step 2. the reactive transport coupling; and finally, Step 3. the phase flow problem, solving Newton's method a second time, considering the phase transfer attributable to the geochemical reactions. This method exerted disadvantageous effects on the convergence and performance because of the delayed treatment of the fluid properties at Step 1. Thus, the gas properties must be implicitly estimated in the iterative loop of flow to guarantee the convergence and unconditional stability, particularly for dominant flow, when the mechanical displacement of the gas front occurs. Consequently, the flow system is fully implicit, and Algorithm 1 inherits its advantages, unlike the time-step restriction of the IMPES method. However, the latter diminishes numerical dispersion and reduces the number of nonlinear equations to be solved simultaneously.

3.4.2. Type of coupling

The sequential coupling of the flow in Algorithm 1 and reactive transport in Algorithm 2 modules has a specific limitation: the flow is supposed to be unreactive. The flow method was initially developed for modeling the gas appearance resulting from mechanical displacement, not the phase transition from the liquid to two-phase state. Nevertheless, within the reactive transport module, the evaporation, dissolution and other chemical processes change the mass of each phase. The impact of such modifications varies with the chemical system of each problem. We manage the changes arising from the RT in the flow block a posteriori by updating the fluid and rock properties and the explicit reaction terms R_α , Eq. (22). This approach is valid if the chemical reaction rates (and their impact on R_α) and time steps remain small; otherwise, the severe changes in the fluid and rock properties hinder the convergence of Newton's method because the initial guess is far from the solution. Because of the explicit treatment, the geochemical impact on the flow can be significantly underestimated. To overcome this problem and model the reaction-driven advection, the tight coupling, similar to the STOMP algorithm (White and Oostrom, 2006), should be applied for high change rates. This strategy allows updating of the velocities and fluid/rock properties implicitly through an iterative procedure involving the flow and SIA-based reactive transport. However, when the mechanical force is dominant, it is computationally efficient to use sequential coupling between the flow and the RT module.

Applying GIA avoids this issue by definition because the phase equilibria are generally calculated at each Newton iteration using the phase stability test (Michelsen, 1982) and thermodynamics flash (Firoozabadi, 1999). The compositional flow system consists of a larger set of nonlinear equations than that of the proposed method. Furthermore, for variable switching, the primary variables should be adapted to the local equilibrium state, which requires reconstructing the Jacobian matrix.

3.4.3. Numerical assessment

Solving the entire problem is divided into two stages: Algorithm 1, the compressible flow coupling composed of N_f nonlinear equations of flow and N_g linear equations of gas transport, followed by Algorithm 2, the reactive transport coupling of $N_c + N_g$ linear transport equations and $N_c + N_{kin}$ nonlinear equations from the chemical system. Let us estimate the computational impact of each part. Assuming a uniform time step for both flow and reactive transport, we denote the calculation time of the entire system t , the flow coupling per iteration t_{flc} , the flow operator t_{fl} , the gas transport t_{gt} and for the reactive transport per iteration t_{rtc} ; then,
$$t = N_{Nit}t_{flc} + N_{Pit}t_{rtc} = N_{Nit}(t_{fl} + t_{gt}) + N_{Pit}t_{rtc}, \quad (30)$$

where N_{Nit} is the number of Newton iterations and N_{Pit} is the number of Picard iterations. Given that $t_{gt} \ll t_{fl}$ and $N_{Pit}t_{rtc} \in (t_{fl}/10^3, N_{Nit}t_{fl})$, we deduce that the calculation time per time step in this process can be expressed as follows

$$N_{Nit}t_{fl} < N_{Nit}t_{fl} + N_{Pit}t_{rtc} \leq 2N_{Nit}t_{fl}. \quad (31)$$

The lower bound corresponds to the problem with a low geochemical complexity (e.g., CO_2 and H_2O). Therefore, the calculation time t is primarily dependent on the flow operator part, and t_{fl} is the controlling factor. This can be reduced using a linear solver and preconditioner (Jiang, 2007) and/or using the AIM for the flow system. The upper limit can be reached when the aggressive geochemistry is modeled with, for example, the (dis-)appearance of solids, gases, and the redox reactions; however, the calculation time t is still strongly dependent on t_{fl} . Thus, we conclude that when the components in the chemical system are more abundant, the proposed flow coupling is more advantageous compared with the methods based on the compositional flow formulation, considering that the larger time stepping in GIA can be compromised by the required reactive time step.

The inner couplings have their own tolerance, which represents another benefit of the OSA: ε_{Nf} and $\varepsilon_g \in [10^{-8}, 10^{-6}]$ for flow, $\varepsilon_{rt} = 10^{-5}$ for reactive transport and 10^{-12} for chemistry; thus, the mass balance error is in the range $[10^{-6}, 10^{-5}]$ according to the test cases used for different types of geochemical and hydrodynamic complexities.

4. Numerical simulations

The proposed method is first tested by modeling a problem with a self-similar solution. Next, we apply it to the simulation of CO_2 injection, allowing the capabilities of the simulator to represent the physical behavior and its computational efficiency to be investigated. Then, an example including mineral reactions is provided.

4.1. 1D axisymmetric problem: Radial flow from a CO_2 injection well

The axisymmetric problem of constant injection in a saturated, horizontal, and infinite reservoir allows the self-similar variable R^2/t , which makes it an ideal approach for verifying the numerical code. In addition, the problem was studied in the workshop "Intercomparison of numerical simulation codes for geologic disposal of CO_2 " initiated by Lawrence Berkeley National Laboratory (Pruess et al., 2002), modeling a constant 100 kg/s CO_2 injection in a long aquifer $100,000 \times 100 \text{ m}^2$. We use the parameters presented in Pruess et al. (2002) and adapt some of them: because the pore compressibility is neglected, we intensify the intrinsic permeability, $K = 2 \times 10^{-13} \text{ [m}^2\text{]}$. Additionally, water is present in each grid cell. The fluid properties and solubility are also treated differently. In HYTEC, the gas and liquid densities are provided by Peng–Robinson models (Ahlers and Gmehling, 2001; Jaubert and Mutelet, 2004; Robinson and Peng, 1978), and the viscosities are

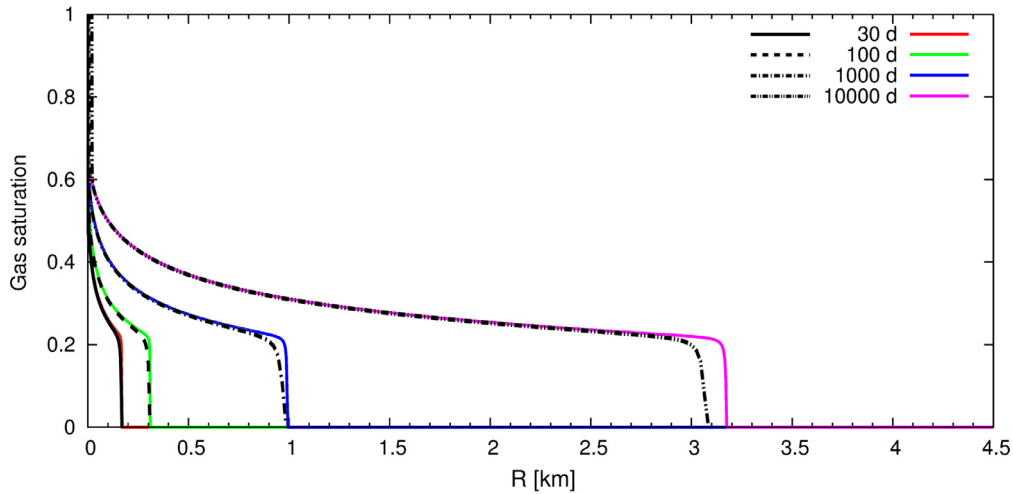


Fig. 1. 1D axisymmetric problem: gas saturation S_g . Results of HYTEC (in color) and TOUGH2-ECO2 (Pruess et al., 2002) (black).

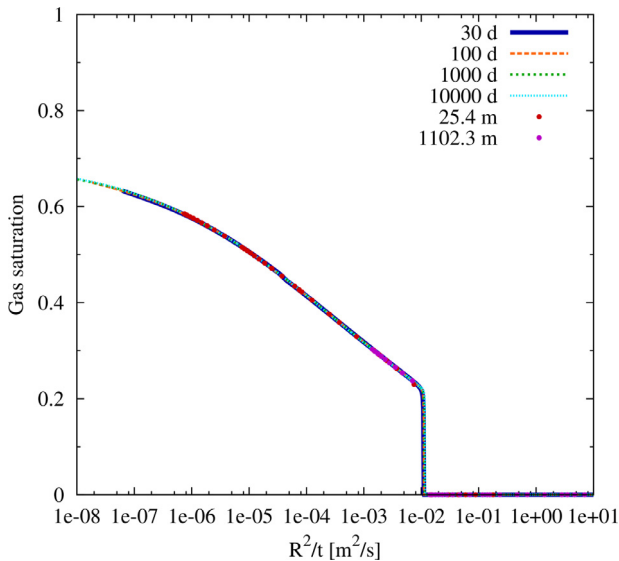


Fig. 2. 1D axisymmetric problem: gas saturation S_g as a function of R^2/t .

predicted by Altunin (1975); Islam and Carlson (2012). The partial molar volume at infinite dilution in water is averaged over the relevant pressure range, and the aqueous activities and gaseous fugacities are simulated according to the b-dot and PR78 (Robinson and Peng, 1978) models, respectively. In Pruess et al. (2002), the TOUGH2-ECO2 module was used, which is described in Pruess and García (2002).

Despite the aforementioned deviation in parameters, the gas saturation front is similar in both cases, particularly over the first 1000 d, as shown in Fig. 1. The increased discrepancy in the saturation front position at 10,000 d arises from the water disappearance zone modeled in Pruess et al. (2002). Note that the saturation curves of HYTEC are almost perpendicular to the R-axis, unlike the slopes of TOUGH2-ECO2, which increase over time because of the truncation errors. The results of gas saturation, presented as a function of R^2/t , are illustrated in Fig. 2 and demonstrate the high accuracy of the numerical code. The results are similar to those obtained by GEM (Computer Modelling Group, 2009) over all modeled domain, Fig. 3(a). Moreover, the gas saturation curve of HYTEC agrees well with those modeled by STOMP, TOUGH2-ECO2 and two modified TOUGH2 except the dry-out zone appeared near the injection well $R^2/t < 5 \times 10^{-6}$ [m²/s], Fig. 3(a). Results for CO₂(aq)

mass-fraction and pressure show a high range of values, Figs. 3(b) and (c). HYTEC provides a lower pressure in a two-phase zone, $R^2/t \leq 10^{-2}$ [m²/s], the pressure relaxation might be caused by the specific treatment of dissolution process in the HYTEC coupling, grid dimension or boundary conditions. The shape of pressure curves and transition zone are still close.

4.2. 2D problem: CO₂ injection in a fully water-saturated domain

The 2D problem of CO₂ injection in a fully water-saturated domain was proposed by Neumann et al. (2013). The CO₂ is injected at a constant rate of 0.04 kg · m⁻² · s⁻¹ through the left bottom boundary (whose length was not provided in Neumann et al. (2013)) of the 600 × 100 m² rectangular reservoir. In this work, the injection border is 10 m long, and thus, the debit is 0.4 kg/s. The Dirichlet boundary conditions are set at the right border of the reservoir: hydrostatic pressure and $S_g = 0$. By neglecting the dispersion and using the Millington-Quirk tortuosity model (Millington and Quirk, 1961), the effective diffusion in this problem takes the following form:

$$D_\alpha^e = \phi^{4/3} S_\alpha^{10/3} D_\alpha. \quad (32)$$

The geometry and grid dimensions are taken from Neumann et al. (2013), whereas the models of fluid properties and solubility (Section 4.1) differ from those used in the reference.

The fluid dynamics is represented exactly as in Neumann et al. (2013): the CO₂ forms a bubble that grows and rises upward. Then, the current is distributed along the top of the aquifer as its area gradually expands, as shown in Fig. 4. The gas saturation is lower than the DUNE results presented in Neumann et al. (2013), whereas the mole fraction of CO₂ in the liquid phase is higher. This might be because of the uncertainty regarding the injection rate used in Neumann et al. (2013) and the different fluid properties and phase equilibria models.

The same grid dimension as in Neumann et al. (2013) is chosen for this simulation: 240 × 40 cells. The maximum number of Newton iterations is set to 9 in HYTEC for this problem. The tolerance of Newton's method (Algorithm 1) is $\epsilon_{Nf} = 10^{-7}$, and the gas quantity criterion Eq. (21) is $\epsilon_g = 10^{-5}$. The mass conservation error is on the order of 10^{-6} .

The initial time step is set to 156 s, which is also the minimum time step $\min(dt)$. The time stepping for HYTEC and DUNE is listed in Table 3. The HYTEC's user-imposed maximum time step $\max(dt)$ is slightly higher (by 8%), and thus, the average dt is larger and the HYTEC is executed faster (by at least 9%).

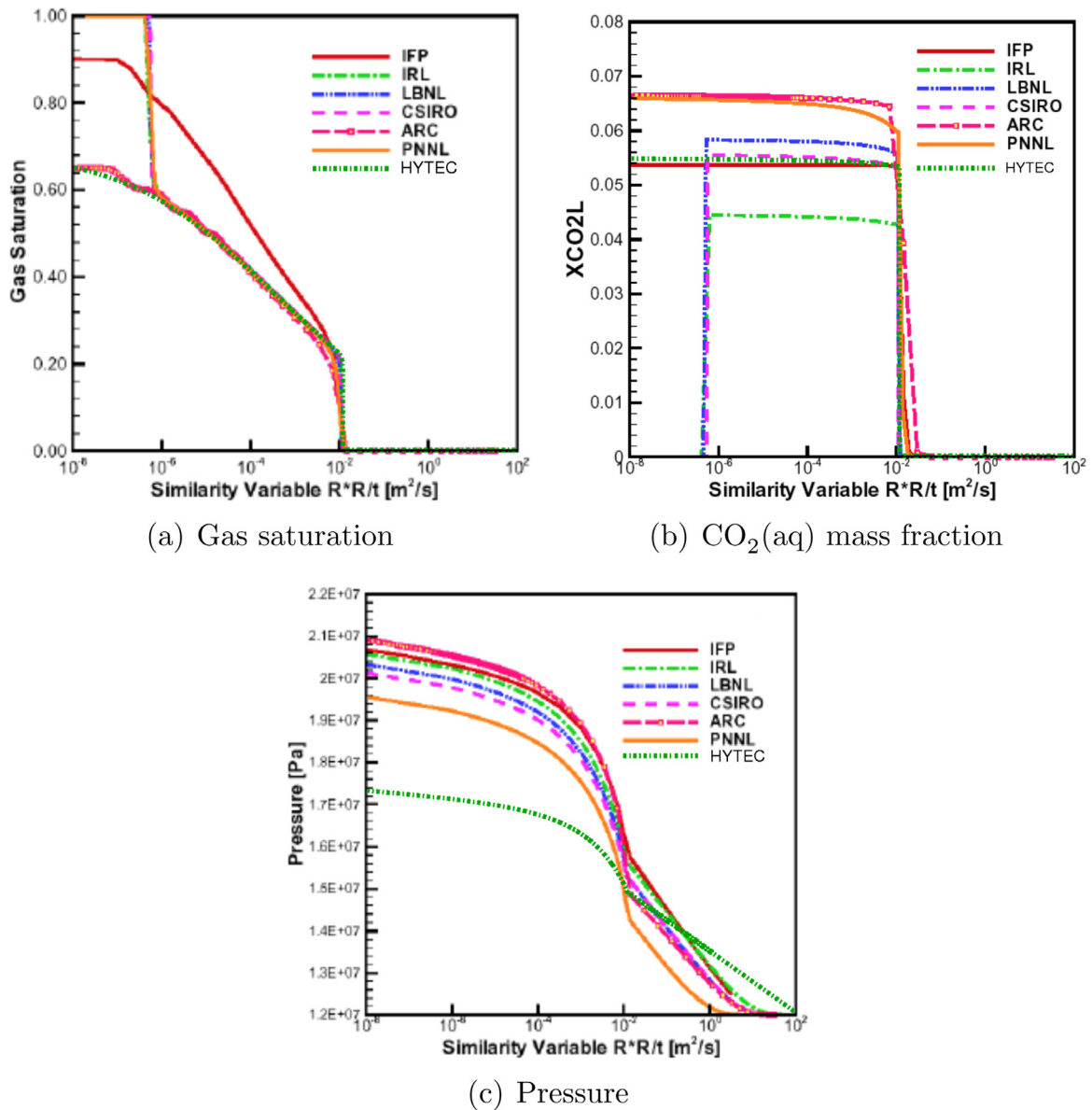


Fig. 3. 1D axisymmetric problem: results obtained by HYTEC and the codes participated in the workshop “Intercomparison of numerical simulation codes for geologic disposal of CO₂” initiated by Lawrence Berkeley National Laboratory (Pruess et al., 2002), where IFP – SIMUSCOPP, IRL, CSIRO – modified TOUGH2, LBNL – TOUGH2-ECO2, ARC – GEM, PNNL – STOMP, (Pruess et al., 2002, Figs. 3.5–3.7).

In Table 4, the HYTEC execution time includes the grid construction, initialization, output printing, solvers, and secondary property modules. During our simulation, the total number of time steps (successful and unsuccessful) was 39% less than that of DUNE, which can be explained by the slightly higher average time step and rate of Newton’s method convergence in HYTEC.

When applying our method, the unsuccessful steps occur immediately after the moment when the gas current reaches the right boundary. Thus, the CO₂(g)’s further propagation is restricted as the dissolved CO₂ is released. Hence, the boundary conditions are no longer adapted to the problem.

4.3. 2D Injection and impact on chemistry

An application is proposed to test the coupling with chemistry. The application builds on the previous 1D radial and 2D injection problems. The gas injection of CO₂ and H₂S takes place in an initially fully saturated reservoir at 3.1 km depth. The reactivity of the host-rock is now taken into account. A homogeneous carbon-

Table 3
2D problem of CO₂ injection in a fully water-saturated domain: time stepping.

	min(dt), s	max(dt), s	mean(dt), s
DUNE	156.25	5,000	3,580
HYTEC	156	5,400	4,475

ated reservoir is simulated: Table 5. All reactions are considered at equilibrium, using the LLNL database (Wolery and Sutton, 2013). Ion and water activity were corrected by the b-dot and Helgeson formalisms (Helgeson, 1969). The Henry’s constants are pressure- and temperature-dependent, the gas-liquid equilibria modeling is described in Section 2.3.2. Sulfur oxidation and sulfate reduction are disabled in this context: the intermediate temperature (80°C) and the relatively short time frame (30 y) do not enable active thermal nor bacterial sulfate reduction (Riciputi et al., 1996; Worden et al., 1996).

The gas injection of 75 mol% of CO₂(g) and 25 mol% of H₂S(g) is modeled at a constant rate of 40 kg/s. The diffusion coefficients

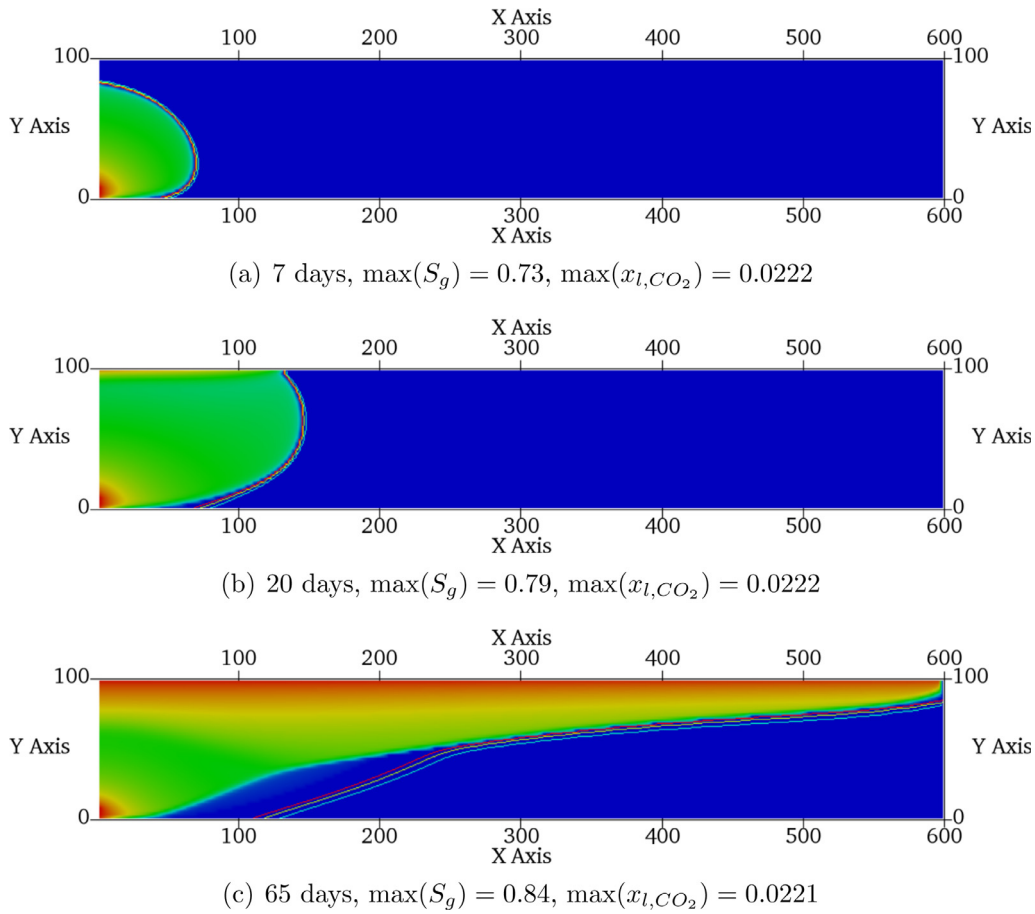


Fig. 4. 2D problem of CO_2 injection in a fully water-saturated domain: gas saturation from $[0, \max(S_g)]$ and contours of CO_2 mole fraction x_{l,CO_2} at 0.005, 0.011, and 0.016.

Table 4

2D problem of CO_2 injection in a fully water-saturated domain: successful and unsuccessful Newton iteration number (Ni), total number of steps (successful and unsuccessful) and total execution time.

	Tot. of time steps	Mean(Ni)	Tot. of Ni	Tot. exec. time, s
DUNE	2,249	3.9	–	13,975
HYTEC	1,380	5.2	7,183	12,708

Table 5

Initial chemical composition of the carbonated reservoir for the fully coupled problem.

	g/L water	g/L rock
Porosity	0.12	
Permeability	10^{-13} m^2	
Calcite	15,170	1,821
Dolomite	3,005	361
Anhydrite	1,029	124
NaCl	150	

in gas and liquid phases are at 7.7×10^{-8} and $5.7 \times 10^{-9} \text{ m}^2/\text{s}$, respectively. The Peng-Robinson EOS (Robinson and Peng, 1978) and McCain model (McCain Jr., 1991) are employed for gas and liquid density modeling. The 100 m-high aquifer is supposed infinite as previously in Section 4.1.

The evolution of gas saturation has already been seen, its shape and displacement are similar to that of 2D problem, Section 4.2. Fig. 5 presents the gas saturation map for the aquifer domain $100 \times 3,000 \text{ m}$ at 30 y, the X-axis is scaled 5:1. However, the gas density distribution in Fig. 6 reveals not only pressure effect but also a heterogeneous behavior at the front of gas current. That physical phenomena, so-called chromatographic partitioning or separation, was experimentally observed in Bachu and Bennion (2009). Fig. 7 illustrates a gas composition at different height of the aquifer. Because CO_2 is less soluble than H_2S and gas current moves forward extending its tongue, accumulation of CO_2 appears ahead, particularly at the top of the aquifer, Fig. 7(a). Slight peaks of $CO_2(\text{aq})$ similar to those of CO_2 in gas

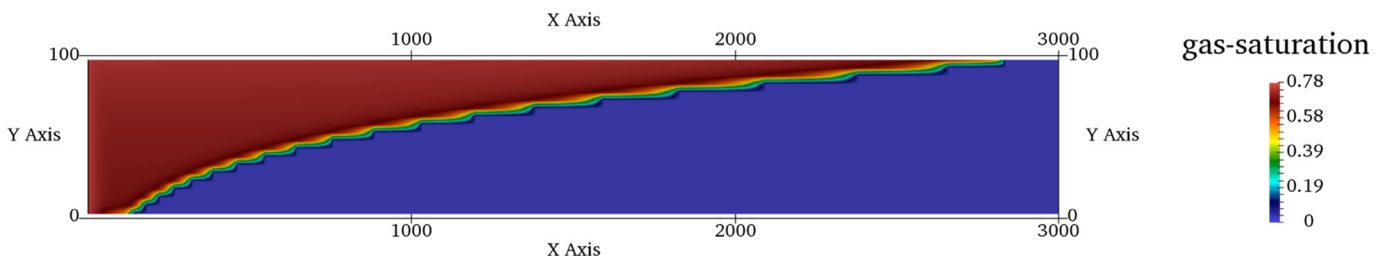


Fig. 5. 2D radial problem: gas saturation at 30 y.

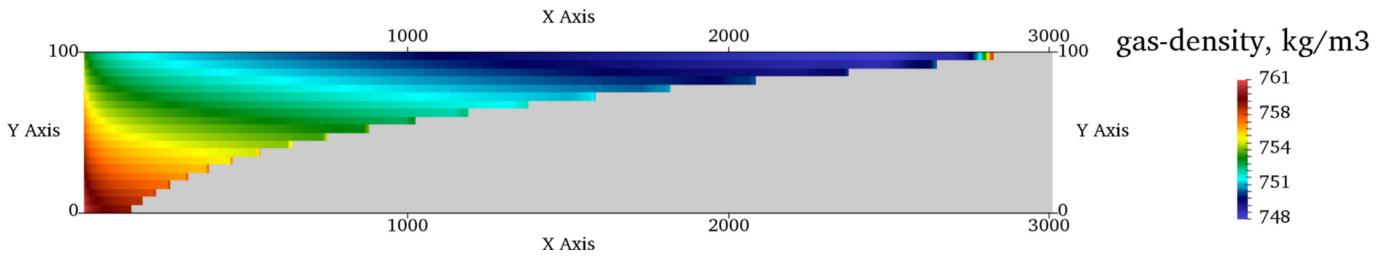
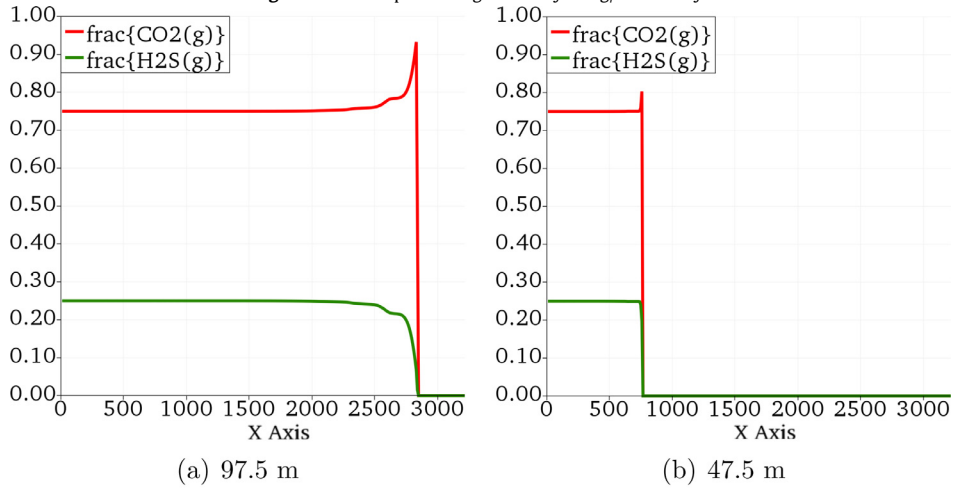
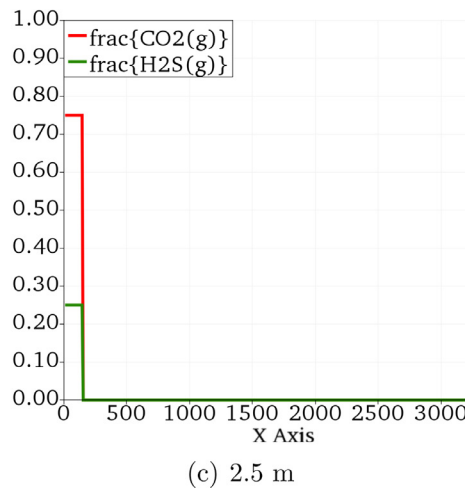


Fig. 6. 2D radial problem: gas density in kg/m³ at 30 y.



(a) 97.5 m

(b) 47.5 m



(c) 2.5 m

Fig. 7. 2D radial problem: mole fractions of CO₂(g) and H₂S(g) at the height (a) 97.5, (b) 47.5 and (c) 2.5 m at 30 y.

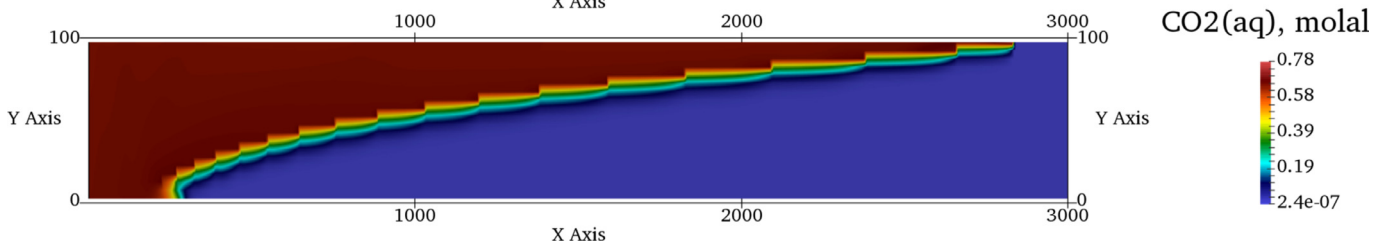


Fig. 8. 2D radial problem: CO₂(aq) concentration in molal at 30 y.

also develop at the front of gas-liquid contact. Figs. 8 and 9 show the concentration map of CO₂(aq) and H₂S(aq) at 30 y, respectively.

The mineralogical evolution is limited. The acid gas injection causes a drop in pH. The carbonate minerals react as pH buffers, and the pH stabilizes from initial 8 to 4.7 within gas dissolution

area, Fig. 10. The mineral dissolution is small due to the buffering: calcite dissolution attains only 0.02%, Fig. 11(a); dolomite dissolution is even less and limited to 0.005%, Fig. 11(b). Indeed, without input of fresh water, the solution reaches an equilibrium with the dissolved calcium, magnesium and carbonate, and prevent further

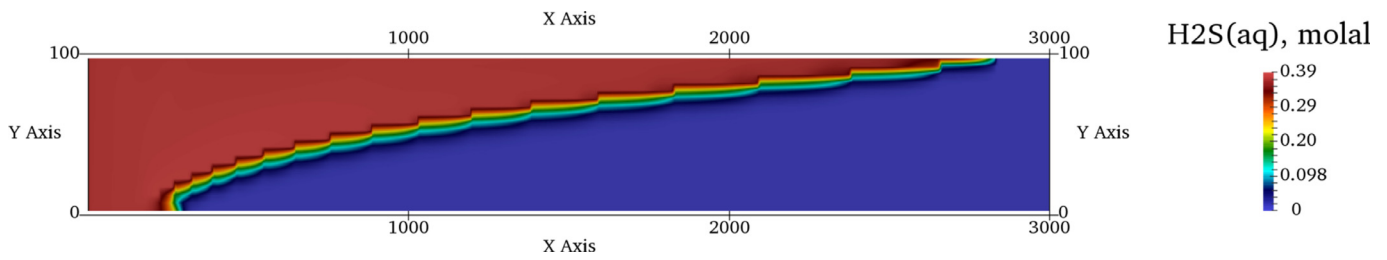


Fig. 9. 2D radial problem: $\text{H}_2\text{S}(\text{aq})$ concentration in molal at 30 y.

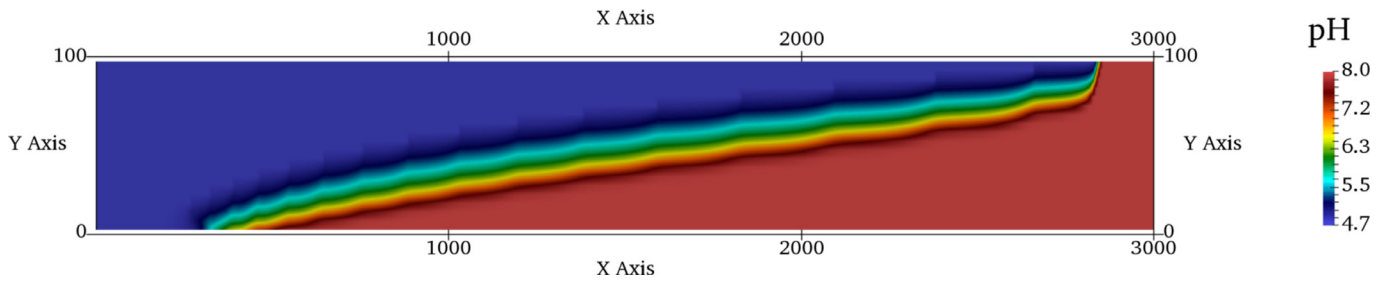
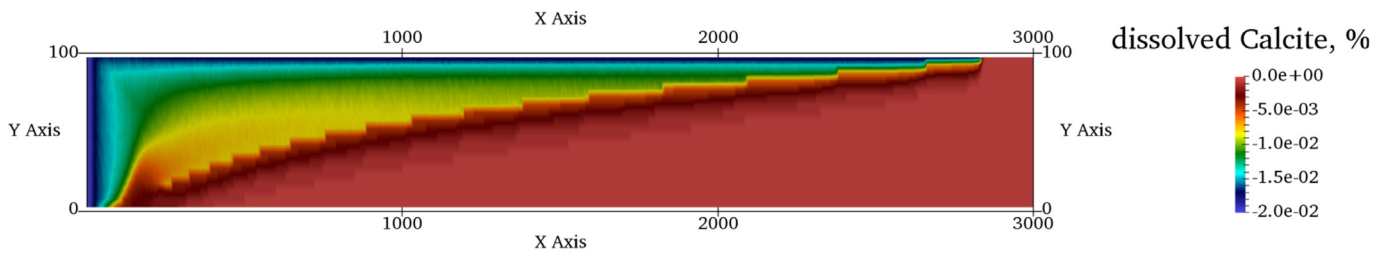
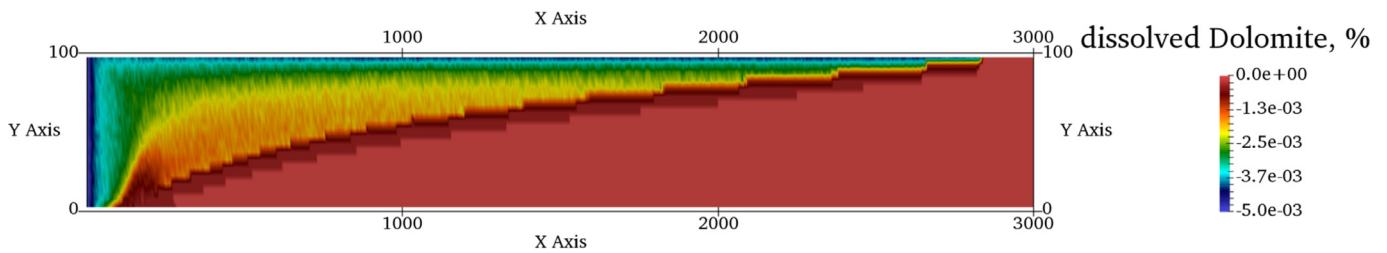


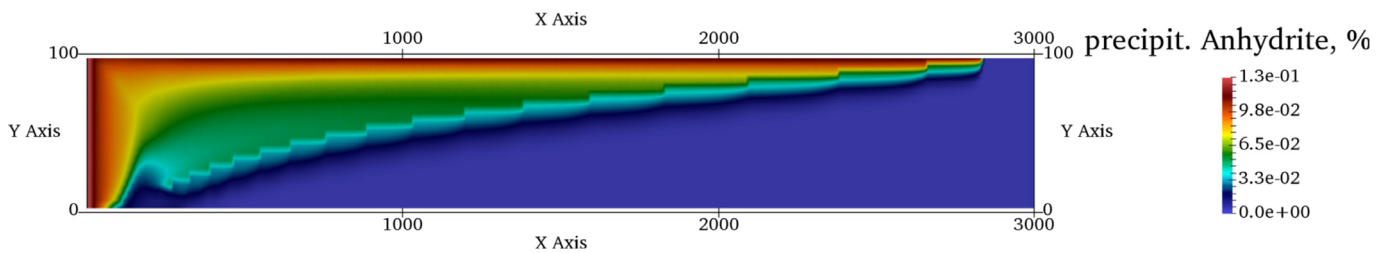
Fig. 10. 2D radial problem: pH at 30 y.



(a) Calcite



(b) Dolomite



(c) Anhydrite

Fig. 11. 2D radial problem: evolution of mineral dissolution in % at 30 y. See text for details.

mineral dissolution. This effect was documented from a chemical-only point of view by Sterpenich et al. (2009).

Finally, without redox reactions between sulfur and sulfate, anhydrite reactivity is limited to small amounts of precipitation (0.1%, Fig. 11(c)), when excess dissolved calcium from the carbonate dissolution reacts with dissolved sulfate.

5. Conclusion

A new solution method for compressible multiphase flow that can be integrated as a module in the OSA- or GIA-based reactive transport frameworks based on the operator splitting or global implicit approach was proposed. The flow method consists of the

phase conservation formulation, the gas transport and the equations of state. This versatile structure allows the constant number of nonlinear equations of the flow problem to be conserved, independent of the geochemical system. Then, in chemistry, the basis components can change during a time step and enhance the convergence. This characteristic makes this method advantageous for modeling multicomponent problems. Furthermore, the entire flow coupling preserves the fully implicit advantages of the multiphase flow discretization.

The present method was implemented in the SIA-based reactive transport simulator HYTEC. The numerical code was verified against a problem accepting a self-similar solution which was documented in an international benchmarking exercise; its computational efficiency was confirmed by simulating CO₂ injection and compared with that of DUNE. The ability to model multiphase multicomponent reactive flow was also demonstrated. Having provided the evidence of the method's capabilities, we note that it needs further validation and verification such as benchmarking of multiphase flow and reactive transport codes to evaluate the impact of coupling approach on modeling physical processes.

Let us discuss the hypotheses assumed in this work. First, the flow problem of water disappearance can be addressed by using alternative formulations of primary variables (e.g., gas pressure/liquid pressure). A rigorous generalization of variable switching is thus possible.

The next issue is the modeling of strongly reactive problems with high geochemical impacts on flow. In this case, the proposed sequential non-iterative coupling between the flow block and the reactive transport block might be insufficient. The method should be analyzed using such cases to evaluate the relevance and efficiency of an iterative approach. Numerical criteria for the possible switching strategy are anticipated. The method's flexibility also allows for its extension to non-isothermal flow. When solving the energy equation, several numerical schemes and coupling algorithms are available. If an explicit discretization is applied for one of the coupling steps, then stability conditions are required.

Acknowledgments

This work was supported by MINES ParisTech and BRGM. I. Sin thanks Christophe Coquelet (Centre for Thermodynamics of Processes, MINES ParisTech) for his insightful suggestions regarding the thermodynamics development and Claude Tadonki (Centre for Computer Science, MINES ParisTech) for productive discussions about linear solvers. We thank three anonymous reviewers for constructive and valuable comments. Their careful analysis helped us significantly improve the manuscript, especially Section 4.

References

Abadpour, A., Panfilov, M., 2009. Method of negative saturations for modeling two-phase compositional flow with oversaturated zones. *Transp. Porous Media* 79 (2), 197–214.

Ahlers, J., Gmehling, J., 2001. Development of an universal group contribution equation of state: I. Prediction of liquid densities for pure compounds with a volume translated Peng–Robinson equation of state. *Fluid Phase Equilib.* 191 (1), 177–188.

Ahusborde, E., Kern, M., Vostrikov, V., 2015. Numerical simulation of two-phase multicomponent flow with reactive transport in porous media: application to geological sequestration of CO₂. *ESAIM: Proc.* 50, 21–39. <http://dx.doi.org/10.1051/proc/201550002>.

Allen, M.B., 1984. Why upwinding is reasonable. *Finite Elem. Water Resour.* 13–23.

Altunin, V., 1975. *The Thermophysical Properties of Carbon Dioxide*. Publishing house of standards, Moscow.

Angelini, O., Chavant, C., Chénier, E., Eymard, R., Granet, S., 2011. Finite volume approximation of a diffusion–dissolution model and application to nuclear waste storage. *Math. Comput. Simul.* 81 (10), 2001–2017.

Aziz, K., Settari, A., 1979. *Petroleum Reservoir Simulation*.

Bachu, S., Bennion, D.B., 2009. Chromatographic partitioning of impurities contained in a CO₂ stream injected into a deep saline aquifer: Part 1. Effects of gas composition and in situ conditions. *Int. J. Greenhouse Gas Control* 3 (4), 458–467.

Bastian, P., 1999. *Numerical Computation of Multiphase Flows in Porous Media*. Christian-Albrechts-Universität Kiel Ph.D. thesis.

Blair, P., Weinaug, C., 1969. Solution of two-phase flow problems using implicit difference equations. *Soc. Pet. Eng. J.* 9 (04), 417–424.

Bourgeat, A., Jurak, M., Smaï, F., 2013. On persistent primary variables for numerical modeling of gas migration in a nuclear waste repository. *Comput. Geosci.* 17 (2), 287–305.

Cao, H., 2002. *Development of Techniques for General Purpose Simulators*. Stanford University Ph.D. thesis.

Carrayrou, J., Hoffmann, J., Knabner, P., Krättele, S., De Dieuleveult, C., Erhel, J., Van Der Lee, J., Lagneau, V., Mayer, K.U., Macquarrie, K.T., 2010. Comparison of numerical methods for simulating strongly nonlinear and heterogeneous reactive transport problems – the MoMaS benchmark case. *Comput. Geosci.* 14 (3), 483–502.

Carrayrou, J., Lagneau, V., 2007. The reactive transport benchmark proposed by GdR MoMaS: presentation and first results. *Eurotherm-81, Reactive Transport Series*, Albi.

Chen, Z., Huan, G., Ma, Y., 2006. *Computational Methods for Multiphase Flows in Porous Media*, Computational Science and Engineering, 2. SIAM, Philadelphia, PA.

Class, H., Helmig, R., Bastian, P., 2002. Numerical simulation of non-isothermal multiphase multicomponent processes in porous media.: 1. An efficient solution technique. *Adv. Water Resour.* 25 (5), 533–550.

Coats, K.H., 1980. An equation of state compositional model. *SPE J.* 20 (5), 363–376.

Colston, B.J., Chandratillake, M.R., Robinson, V.J., 1990. Correction for Ionic Strength Effects in Modelling Aqueous Systems. NIREX.

Corvisier, J., Bonvalot, A., Lagneau, V., Chiquet, P., Renard, S., Sterpenich, J., Pironon, J., 2013. Impact of co-injected gases on CO₂ storage sites: geochemical modeling of experimental results. In: *Proceedings of the International Conference on Greenhouse Gas Technology 11, Kyoto*. Energy Procedia, pp. 3699–3710.

Computer Modelling Group, 2009. *User's Guide GEM: Advanced Compositional and GHG Reservoir Simulator*. Calgary, Canada.

Debure, M., de Windt, L., Frugier, P., Gin, S., 2013. HLW Glass dissolution in the presence of magnesium carbonate: diffusion cell experiment and coupled modeling of diffusion and geochemical interactions. *J. Nucl. Mater.* 443, 507–521.

Delshad, M., Pope, G., Sepehrnoori, K., 2000. *UTCHEM Version 9.0 Technical Documentation*. Technical Report. Center for Petroleum and Geosystems Engineering, The University of Texas at Austin, Austin, Texas, 78751.

de Dieuleveult, C., 2008. *Un modèle numérique global et performant pour le couplage géochimie-transport*. Rennes 1 Ph.D. thesis.

de Dieuleveult, C., Erhel, J., Kern, M., 2009. A global strategy for solving reactive transport equations. *J. Comput. Phys.* 228 (17), 6395–6410.

Fan, Y., Durlöfsky, L.J., Tchelepi, H.A., 2012. A fully-coupled flow-reactive-transport formulation based on element conservation, with application to CO₂ storage simulations. *Adv. Water Resour.* 42, 47–61.

Farajzadeh, R., Matsuura, T., van Batenburg, D., Dijk, H., 2012. Detailed modeling of the alkali/surfactant/polymer (asp) process by coupling a multipurpose reservoir simulator to the chemistry package PHREEQC. *SPE Reservoir Eval. Eng.* 15 (04), 423–435.

Firoozabadi, A., 1999. *Thermodynamics of Hydrocarbon Reservoirs*. McGraw-Hill, New York.

Gamazo, P., Saaltink, M.W., Carrera, J., Slooten, L., Bea, S., 2012. A consistent compositional formulation for multiphase reactive transport where chemistry affects hydrodynamics. *Adv. Water Resour.* 35, 83–93.

Grenthe, I., Plyasunov, A.V., Spahiu, K., 1997. Estimations of medium effects on thermodynamic data. *Model. Aquatic Chem.* 325.

Hao, Y., Sun, Y., Nitaou, J., 2012. Overview of NUFF: a versatile numerical model for simulating flow and reactive transport in porous media. *Groundw. Reactive Transp. Models* 212–239.

Helgeson, H.C., 1969. Thermodynamics of hydrothermal systems at elevated temperatures and pressures. *Am. J. Sci.* 267 (7), 729–804.

Hoteit, H., 2011. Proper modeling of diffusion in fractured reservoirs. *SPE Reservoir Simulation Symposium*. Society of Petroleum Engineers.

Hoteit, H., Firoozabadi, A., 2006. Compositional modeling by the combined discontinuous Galerkin and mixed methods. *SPE J.* 11 (01), 19–34.

Hron, P., Jost, D., Bastian, P., Gallert, C., Winter, J., Ippisch, O., 2015. Application of reactive transport modeling to growth and transport of microorganisms in the capillary fringe. *V. Vadose Zone J.* 14 (5).

Islam, A.W., Carlson, E.S., 2012. Viscosity models and effects of dissolved CO₂. *Energy & Fuels* 26 (8), 5330–5336.

Jacquemet, N., Pironon, J., Lagneau, V., Saint-Marc, J., 2012. Armouring of well cement in H₂S-CO₂ saturated brine by calcite coating-experiments and numerical modeling. *Appl. Geochem.* 27, 782–795.

Jaubert, J.-N., Mutelet, F., 2004. VLE Predictions with the Peng–Robinson equation of state and temperature dependent kij calculated through a group contribution method. *Fluid Phase Equilib.* 224 (2), 285–304.

Jiang, Y., 2007. *Techniques for Modeling Complex Reservoirs and Advanced Wells*. Stanford University Ph.D. thesis.

Jindrová, T., Mikyška, J., 2015. General algorithm for multiphase equilibria calculation at given volume, temperature, and moles. *Fluid Phase Equilib.* 393, 7–25.

Krättele, S., Knabner, P., 2007. A reduction scheme for coupled multicomponent transport–reaction problems in porous media: generalization to problems with heterogeneous equilibrium reactions. *Water Resour. Res.* 43 (3).

Lagneau, V., van der Lee, J., 2010a. HYTEC results of the MoMaS reactive transport benchmark. *Comput. Geosci.* 14 (3), 435–449.

- Lagneau, V., van der Lee, J., 2010b. Operator-splitting-based reactive transport models in strong feedback of porosity change: the contribution of analytical solutions for accuracy validation and estimator improvement. *J. Contam. Hydrol.* 112 (1), 118–129.
- Lagneau, V., Pipart, A., Catalette, H., 2005. Reactive transport modelling of CO₂ sequestration in deep saline aquifers. *Oil Gas Sci. Technol.* 60, 231–247.
- Lasaga, A.C., 1984. Chemical kinetics of water-rock interactions. *J. Geophys. Res.: Solid Earth* (1978–2012) 89 (B6), 4009–4025.
- Lauser, A., Hager, C., Helmig, R., Wohlmuth, B., 2011. A new approach for phase transitions in miscible multi-phase flow in porous media. *Adv. Water Resour.* 34 (8), 957–966.
- van der Lee, J., 2009. Thermodynamic and Mathematical Concepts of CHESST-20093103-JVDL. Technical Report. École des Mines de Paris, Centre de Géosciences, Fontainebleau, France.
- van der Lee, J., de Windt, L., Lagneau, V., Goblet, P., 2003. Module-oriented modeling of reactive transport with HYTEC. *Comput. Geosci.* 29 (3), 265–275.
- Lichtner, P., 1996. Continuum formulation of multicomponent–multiphase reactive transport. *Rev. Mineral.* 34: Reactive Transport in Porous Media, 1–81.
- Lichtner, P., Hammond, G., Lu, C., Karra, S., Bisht, G., Andre, B., Mills, R., Kumar, J., 2015. PFLORAN User Manual: A massively parallel reactive flow and transport model for describing surface and subsurface processes. Technical Report LA-UR-15-20403, 2015, Los Alamos Natl. Lab., Los Alamos, N. M.
- Lu, C., Lichtner, P.C., 2007. High resolution numerical investigation on the effect of convective instability on long term CO₂ storage in saline aquifers. *J. Phys.: Conf. Ser. IOP Publishing.* 78 (1), 012042. <http://dx.doi.org/10.1088/1742-6596/78/1/012042>.
- de Marsily, G., 2004. Cours D'hydrogéologie. Université Paris VI.
- Masson, R., Trenty, L., Zhang, Y., 2014. Formulations of two phase liquid gas compositional darcy flows with phase transitions. *Int. J. Finite* 11, 34.
- Mayer, K., Amos, R., Molins, S., Gérard, F., 2012. Reactive transport modeling in variably saturated media with MIN3p: basic model formulation and model enhancements. In: Zhang, F., Yeh, G.T., Parker, J.C., Shi, X. (Eds.), *Groundwater reactive transport models*. Bentham Science Publishers Ltd., pp. 186–211.
- McCain Jr., W., 1991. Reservoir-fluid property correlations-state of the art. *SPE Reservoir Eng.* 6 (02), 266–272.
- Michelsen, M.L., 1982. The isothermal flash problem. Part I. Stability. *Fluid Phase Equilib.* 9 (1), 1–19.
- Michelsen, M.L., Mollerup, J., 2007. Thermodynamic Models: Fundamentals & Computational Aspects, 2 Tie-Line Publications, Denmark.
- Mikyška, J., Firoozabadi, A., 2010. Implementation of higher-order methods for robust and efficient compositional simulation. *J. Comput. Phys.* 229 (8), 2898–2913.
- Millington, R., Quirk, J., 1961. Permeability of porous solids. *Trans. Faraday Soc.* 57, 1200–1207.
- Molins, S., Carrera, J., Ayora, C., Saaltink, M.W., 2004. A formulation for decoupling components in reactive transport problems. *Water Resour. Res.* 40 (10), 13.
- Molins, S., Mayer, K., 2007. Coupling between geochemical reactions and multicomponent gas and solute transport in unsaturated media: A reactive transport modeling study. *Water Resour. Res.* 43 (5), 16.
- Morel, F., Hering, J., 1993. Principles and Applications of Aquatic Chemistry. John Wiley & Sons, New York.
- Muskat, M., Wyckoff, R., Botset, H., Meres, M., 1937. Flow of gas-liquid mixtures through sands. *Trans. AIME* 123 (01), 69–96.
- Nardi, A., Idiart, A., Trincherio, P., de Vries, L.M., Molinero, J., 2014. Interface COM-SOL-PHREEQC (iCP), an efficient numerical framework for the solution of coupled multiphysics and geochemistry. *Comput. Geosci.* 69, 10–21.
- Neumann, R., Bastian, P., Ippisch, O., 2013. Modeling and simulation of two-phase two-component flow with disappearing nonwetting phase. *Comput. Geosci.* 17 (1), 139–149.
- Nghiêm, L., Sammon, P., Grabenstetter, J., Ohkuma, H., 2004. Modeling CO₂ storage in aquifers with a fully-coupled geochemical EOS compositional simulator. In: *Proceedings of SPE/DOE Symposium on Improved Oil Recovery*. Society of Petroleum Engineers.
- Olivella, S., Gens, A., Carrera, J., Alonso, E., 1996. Numerical formulation for a simulator (CODE_BRIGHT) for the coupled analysis of saline media. *Eng. Comput.* (Swansea) 13 (7), 87–112.
- Parkhurst, D.L., Appelo, C.A.J., 1999. User's Guide to PHREEQC (Version 2): A computer program for speciation, batch-reaction, one-dimensional transport, and inverse geochemical calculations. US Geological Survey Denver, CO.
- Peszyńska, M., Sun, S., 2002. Reactive transport model coupled to multiphase flow models. In: Hassanizadeh, S.M., Schotting, R.J., Gray, W.G., Pinder, G.F. (Eds.), *Computational Methods in Water Resources*. Elsevier, pp. 923–930.
- Pitzer, K., 1991. Ion interaction approach: theory and data correlation. *Activity Coeff. Electrolyte Solut.* 2, 75–153.
- Pope, G.A., Sepehrnoori, K., Delshad, M., 2005. A new generation chemical flooding simulator. Technical Report. Center for Petroleum and Geosystems Engineering, The University of Texas at Austin.
- Pruess, K., García, J., 2002. Multiphase flow dynamics during CO₂ injection into saline aquifers. *Environ. Geol.* 42, 282–295.
- Pruess, K., García, J., Kovscek, T., Oldenburg, C., Rutqvist, J., Steefel, C., Xu, T., 2002. Intercomparison of Numerical Simulation Codes for Geologic Disposal of CO₂. Report LBNL-51813. Lawrence Berkeley National Laboratory, Berkeley, CA 94720.
- Pruess, K., Oldenburg, C., Moridis, G., 1999. TOUGH2 User's Guide, Version 2.0.
- Regnault, O., Lagneau, V., Fiet, O., 2014. 3D Reactive transport simulations of uranium in situ leaching: forecast and process optimization. In: Merkel, B., Arab, A. (Eds.), *Proceedings of the 7th International Conference on Uranium Mining and Hydrogeology*, Sept 21–25 2014, Freiberg, Germany., pp. 725–730.
- Riciputi, L., Cole, D., Machel, H., 1996. Sulfide formation in reservoir carbonates of the Devonian Nisku formation, Alberta, Canada: An ion microprobe study. *Geochim. Cosmochim. Acta* 60, 325–336.
- Robinson, D.B., Peng, D.-Y., 1978. The Characterization of the Heptanes and Heavier Fractions for the GPA Peng-Robinson Programs. Technical Report.
- Saad, Y., Schultz, M.H., 1986. GMRES: A generalized minimal residual algorithm for solving nonsymmetric linear systems. *SIAM J. Sci. Stat. Comput.* 7 (3), 856–869.
- Saaltink, M.W., Ayora, C., Carrera, J., 1998. A mathematical formulation for reactive transport that eliminates mineral concentrations. *Water Resour. Res.* 34 (7), 1649–1656.
- Saaltink, M.W., Carrera, J., Ayora, C., 2001. On the behavior of approaches to simulate reactive transport. *J. Contam. Hydrol.* 48 (3), 213–235.
- Saaltink, M.W., Battle, F., Ayora, C., Carrera, J., Olivella, S., 2004. RETRASO, a code for modeling reactive transport in saturated and unsaturated porous media. *Geologica Acta* 2 (3), 235.
- Saaltink, M.W., Vilarasa, V., De Gaspari, F., Silva, O., Carrera, J., Rötting, T.S., 2013. A method for incorporating equilibrium chemical reactions into multiphase flow models for CO₂ storage. *Adv. Water Resour.* 62, 431–441.
- Settari, A., Aziz, K., 1975. Treatment of nonlinear terms in the numerical solution of partial differential equations for multiphase flow in porous media. *Int. J. Multiphase Flow* 1 (6), 817–844.
- Steefel, C., 2009. Crunch flow software for modeling multicomponent reactive flow and transport. User's manual. Earth Sciences Division. Lawrence Berkeley, National Laboratory, Berkeley, CA., pp. 12–91.
- Steefel, C., Appelo, C.A.J., Arora, B., Jacques, D., Kalbacher, T., Kolditz, O., Lagneau, V., Lichtner, P., Mayer, K., Meeussen, J.C.L., 2014. Reactive transport codes for subsurface environmental simulation. *Comput. Geosci.* 1–34. <http://dx.doi.org/10.1007/s10596-014-9443-x>.
- Steefel, C., MacQuarrie, K.T., 1996. Approaches to modeling of reactive transport in porous media. *Rev. Mineral.* 34, 83–129. Reactive Transport in Porous Media
- Sterpenich, J., Sausse, J., Pironon, J., Géhin, A., Hubert, G., Perfetti, E., Grgic, D., 2009. Experimental ageing of oolitic limestones under CO₂ storage conditions: petrographical and chemical evidence. *Chem. Geol.* 265 (1), 99–112. <http://dx.doi.org/10.1016/j.chemgeo.2009.04.011>.
- Trotignon, L., Didot, A., Bildstein, O., Lagneau, V., Margerit, Y., 2005. Design of a 2-D cementation experiment in porous medium using numerical simulation. *Oil & Gas Sci. Technol.* 60 (2), 307–318.
- van der Vorst, H., Meijerink, J., 1981. Guidelines for the usage of incomplete decompositions in solving sets of linear equations as they occur in practical problems. *J. Comput. Phys.* 44 (1), 134–155.
- Vostrikov, V., 2014. Numerical Simulation of Two-Phase Multicomponent Flow with Reactive Transport in Porous Media. Université de Pau et des Pays de l'Adour Ph.D. thesis.
- Wang, P., Yotov, I., Wheeler, M., Arbogast, T., Dawson, C., Parashar, M., Sepehrnoori, K., 1997. A new generation EOS compositional reservoir simulator: Part I-formulation and discretization. SPE Reservoir Simulation Symposium. Society of Petroleum Engineers.
- Wei, L., 2012. Sequential coupling of geochemical reactions with reservoir simulations for waterflood and EOR studies. *SPE J.* 17 (02), 469–484.
- Wheeler, M., Sun, S., Thomas, S., 2012. Modeling of Flow and Reactive Transport in IPARS. Bentham Science Publishers Ltd. <http://dx.doi.org/10.2174/978160805306311201010042>.
- White, M., Bacon, D., McGrail, B., Watson, D., White, S., Zhang, Z., 2012. STOMP Subsurface Transport Over Multiple Phases: STOMP-CO₂ and STOMP-CO₂E Guide: Version 1.0, PNNL-21268 Pacific Northwest National Laboratory, Richland, WA.
- White, M., Oostrom, M., 2006. STOMP Subsurface Transport over Multiple Phases, Version 4.0, User's Guide, PNNL-15782 Pacific Northwest National Laboratory, Richland, WA.
- de Windt, L., Burnol, A., Montarnal, P., Van Der Lee, J., 2003. Intercomparison of reactive transport models applied to UO₂ oxidative dissolution and uranium migration. *J. Contam. Hydrol.* 61 (1), 303–312.
- de Windt, L., Devillers, P., 2010. Modeling the degradation of portland cement pastes by biogenic organic acids. *Cem. Concr. Res.* 40, 1165–1174.
- de Windt, L., Marsal, F., Corvisier, J., Pellegrini, D., 2014. Modeling of oxygen gas diffusion and consumption during the oxidic transient in a disposal cell of radioactive waste. *Appl. Geochem.* 41, 115–127.
- Wolery, T., Sutton, M., 2013. Evaluation of Thermodynamic Data. Technical Report 640133. Lawrence Livermore National Laboratory (LLNL), Livermore, CA, USA.
- Worden, R., Smalley, P., Oxtoby, N., 1996. The effects of thermochemical sulfate reduction upon formation water salinity and oxygen isotopes in carbonate gas reservoirs. *Geochim. et Cosmochim. Acta* 60, 3925–3931.
- Xu, T., Pruess, K., 1998. Coupled Modeling of Non-isothermal Multiphase Flow, Solute Transport and Reactive Chemistry in Porous and Fractured Media: 1. Model Development and Validation.. Lawrence Berkeley National Laboratory. URL <http://escholarship.org/uc/item/9p64p400>.
- Xu, T., Spycher, N., Sonnenthal, E., Zheng, L., Pruess, K., 2012. TOUGHREACT User's Guide: a Simulation Program for Non-isothermal Multiphase Reactive Transport in Variably Saturated Geologic Media, Version 2.0. Earth Sciences Division, Lawrence Berkeley National Laboratory, Berkeley, USA.

- Yeh, G., Sun, J., Jardine, P., Burgos, W., Fang, Y., Li, M., Siegel, M., 2004. HYDROGEOCHEM 5.0: A Three-dimensional Model of Coupled Fluid Flow, Thermal Transport, and Hydrogeochemical Transport through Variably Saturated Conditions. Version 5.0. ORNL/TM-2004/107, Oak Ridge National Laboratory, Oak Ridge, TN.
- Yeh, G., Tripathi, V., 1991. A model for simulating transport of reactive multi-species components: model development and demonstration. *Water Resour. Res.* 27, 3075–3094.
- Yeh, G., Tripathi, V., Gwo, J., Cheng, H., Cheng, J., Salvage, K., Li, M., Fang, Y., Li, Y., Sun, J., Zhang, F., Siegel, M.D., 2012. HYDROGEOCHEM: A coupled model of variably saturated flow, thermal transport, and reactive biogeochemical transport. *Groundw. Reactive Transp. Models* 3–41.
- Zidane, A., Firoozabadi, A., 2015. An implicit numerical model for multicomponent compressible two-phase flow in porous media. *Adv. Water Resour.* 85, 64–78.